Electric Vehicles Charging Management System for Optimal Exploitation of Photovoltaic Energy Sources Considering Vehicle-to-Vehicle Mode

Francesco Lo Franco[1], Riccardo Mandrioli[1], Mattia Ricco[1]*, Vítor Monteiro[2], Luís F. C. Monteiro[3], João L. Afonso[2] and Gabriele Grandi[1]

[1]Department of Electrical, Electronic, and Information Engineering, University of Bologna, Bologna, Italy, [2]Department of Industrial Electronics, Centro ALGORITMI, University of Minho, Guimarães, Portugal, [3]Department of Electronics and Telecommunications, Rio de Janeiro State University, Rio de Janeiro, Brazil

The growing penetration of distributed renewable energy sources (RES) together with the increasing number of new electric vehicle (EV) model registrations is playing a significant role in zero-carbon energy communities' development. However, the ever-larger share of intermittent renewable power plants, combined with the high and uncontrolled aggregate EV charging demand, requires an evolution toward new planning and management paradigms of energy districts. Thus, in this context, this paper proposes novel smart charging (SC) techniques that aim to integrate as much as possible RES generation and EV charging demand at the local level, synergically acting on power flows and avoiding detrimental effects on the electrical power system. To make this possible, a centralized charging management system (CMS) capable of individually modulating each charging power of plugged EVs is presented in this paper. The CMS aims to maximize the charging self-consumption from local RES, flattening the peak power required to the external grid. Moreover, the CMS guarantees an overall good state of charge (SOC) at departure time for all the vehicles without requiring additional energy from the grid even under low RES power availability conditions. Two methods that differ as a function of the EV power flow direction are proposed. The first SC only involves unidirectional power flow, while the second one also considers bidirectional power flow among vehicles, operating in vehicle-to-vehicle (V2V) mode. Finally, simulations, which are presented considering an actual case study, validate the SC effects on a reference scenario consisting of an industrial area having a photovoltaic (PV) plant, non-modulable electrical loads, and EV charging stations (CS). Results are collected and performance improvements by operating the different SC methods are compared and described in detail in this paper.

Keywords: electric vehicles, smart charging, vehicle-to-vehicle (V2V), renewable energy source (RES), state of charge (SOC), photovoltaic (PV), parking lot charging station, charging management system (CMS)

INTRODUCTION

Renewable energy sources (RESs), together with electric vehicles (EVs), constitute one of the main points in the green energy shift toward a less carbon-dependent society (Directorate-General for Climate Action (European Commission), 2019). On this matter, particular attention is dedicated to the growing context of positive energy districts (PEDs) to reduce carbon emissions coming from urban areas (Hinterberger et al., 2020; Tuominen, 2020; Rancilio et al., 2021). The general purpose of PED is to be a flexible part of the whole energy system organized in districts rather than single buildings, ensuring an energy exchange between the various stakeholders (Mirbagheri et al., 2018; Tuominen, 2020). A similar paradigm can resemble a net-zero-energy community (ZEC) where renewable energy matches electrical loads, thermal energy consumption, and EVs charging demand (Dogan et al., 2015; Lopes et al., 2016; Zatti et al., 2017).

However, it has been highlighted that replacing conventional vehicles with electric counterparts would sharply increase peak demand forcing a relevant rethinking of the generation, transmission, and distribution system with significant investment already at moderate levels of EV penetration (Nelder and Fitzgerald, 2016; Bovera et al., 2021). A similar concern is caused by the intermittent nature of RES, whose power generation strongly depends on the availability of the primary source (wind, solar, etc.) and cannot usually provide the control and regulation services that conventional sources can do (Luo and Ooi, 2006; Kroposki et al., 2017; Lo Franco et al., 2021a). Intermittent power injection together with localized load power peaks (aggregate EV charging) might even bring to the nonoptimal utilization of conventional plannable power sources for grid supporting operation (ancillary services). However, since conventional generation methods are fossil fuel reliant, this phenomenon is in contrast to the green policy that characterizes the PED, ZEC, and in general RES and EV development. It stands clear that, for mitigating efforts, detrimental effects, and expensive expedients, a synergic integration of EVs with RES (especially photovoltaic (PV)) is an imperative requirement for future smart power systems (Aldik and Khatib, 2019; Hasan et al., 2019; Rakhshani et al., 2019). Indeed, unmanaged grid-to-vehicle (G2V) charging technique is recognized for not being a long-term economically sustainable option, and the development of vehicle-to-anything (V2X) alternatives has been presented as a possible sustainable solution to this issue (Ferreira et al., 2014; Thompson and Perez, 2020). The umbrella term V2X is often used for indicating any unidirectional (V1X) or bidirectional (the actual meaning of V2X) charging management system (CMS) aiming to provide benefits like peak reduction, load shifting, and flattening together with RES self-consumption optimization (Thompson, 2018; Pearre and Ribberink, 2019). Some of the prevailing techniques are vehicle-to-grid (V2G), vehicle-to-building (V2B), vehicle-to-load (V2L), and vehicle-to-community (V2C) (Monteiro et al., 2016). Among them, V2G constitutes by far the most focused method because of the tremendous potential benefits guaranteed by energy and ancillary services that the interaction between EV batteries and the grid might

unlock (Lopes et al., 2011; Hasan et al., 2019; Noel et al., 2021). Similar to V2X, V2G presents a unidirectional subset referred to as V1G or more often as smart charging (SC). However, the highly sophisticated real-time communication and control backbone necessary for providing grid services has not reached an adequate technological maturity, and only a small number of commercial products are available yet (Thingvad et al., 2016; Zipf and Most, 2016).

For this reason, multiple authors proposed CMSs capable of providing the above benefits at a local level without necessarily involving the active interaction with the grid and all the associated technological challenges (Bons et al., 2020; Lo Franco et al., 2020). These SC systems, mainly if employed over an aggregate EV fleet, blend particularly well with the definitions of V2B and V2C (Thompson, 2018; Noel et al., 2019). Indeed, taking advance of the capacity made available by aggregated EV fleets, it is possible to optimize the energy consumption of the buildings, mainly in the commercial and industrial context, and energy communities by acting solely at the local value (Yamagata et al., 2014; Tanguy et al., 2016). Although a centralized controller capable of communicating with all the vehicles and charging equipment is still required, its complexity results to be noticeably lower if compared to the V2G mode. Finally, V2L can be simplistically defined as any EV (or aggregates) supplying generic loads, including EVs themselves (Thompson and Perez, 2020). For this reason, it is generally accepted vehicle-to-vehicle (V2V) technique to be a particular case of V2L (Mao et al., 2018). In this case, EVs can act as an energy source for supplying other EVs, pursuing a determined charging policy at a local level. Since there is no sharp edge between all these technologies, it would not be surprising if CMS strategies might achieve specific V2B/V2C and V2V optimizations, especially if considered in contexts, like PEDs, presenting internal generation from RES.

Multiple SC methods have been presented in the literature (Wang et al., 2016; Fachrizal and Munkhammar, 2020; Fouladi et al., 2020; Lo Franco et al., 2020). The list below compares the achieved results of some main reference papers and points out the literature gap that this work tries to fill:

- Authors in (Wang et al., 2016) discussed a strategy for achieving flat power demand employing peak-shaving and valley-filling techniques considering cost minimization constraints. This reference provides a survey from the algorithmic perspective. However, a qualitative and quantitative analysis of the SC benefit based on actual case studies has not been provided. The integration of EV charging with RES considering a variegated population of EV model and the capability of bidirectional power flow among vehicles has not been investigated in this reference.

- In (Fachrizal and Munkhammar, 2020; Ramadhani et al., 2021), the authors investigate the probabilistic impact of EV SC, including the temporal and spatial variability of EV charging demand, household load, and PV system generation. The conclusions show that SC results in improved distribution system performance. Although this

reference paper provides an estimation of EV power load considering quantitative data analyses, the PV-EV system integration under low irradiance availability and SC strategies involving the bidirectionality of EV power flow have not been evaluated.

- Three different SC strategies to increase PV solar exploitation are proposed in (Heinisch et al., 2021). The results show that SC strategies can increase up to 62% of the share of PV energy in the charging energy mix, compared to 24% obtained using standard G2V charging. However, this work does not consider a variegate population of EVs, to which different models with different specifications and characteristics belong (such as vehicle battery sizes, onboard charger ratings, and battery state of charge (SOC) at the beginning of the charging process). Moreover, considerations of the SC performance under low PV power conditions are not provided.
- SC methods for self-consumption optimization have been performed in (Lo Franco et al., 2020) employing CMSs capable of modulating each EV charging power individually to industrial districts. This work quantitatively analyzes EV power demand based on a statistical approach and using actual data. However, although self-consumption improvement and peak load reduction are achieved, the proposed CMS does not provide enough energy to the vehicle when low PV availability occurs, leading to a lower EVs' SOC at the end of the charging process (nonoptimal exploitation of PV sources). Also, bidirectional EV power flows capability has not been considered.
- A preliminary solution was provided in (Lo Franco et al., 2021b), where the proposed CMS differently allocates the available PV energy among charging vehicles as a function of the irradiance availability. Although the results show improved performance in terms of EVs' SOC at the end of charging, even this paper does not consider the possibility of power-sharing among vehicles given by the bidirectional V2V mode.

Finally, to the best of the authors' knowledge, no work provides a CMS capable of modulating each EV charging power to optimally exploit the intermittent PV source under low irradiance condition guaranteeing an appreciable trade-off between self-consumption improvement, peak load reduction, and overall good SOC level at the departure time, and in addition, it is also capable of involving power-sharing among vehicle at the local level (bidirectional V2V charging mode). To overcome the aforementioned limitations, two novel charging strategies are proposed in this paper to improve the EV charging process by differently and smartly allocating the available RES power to each EV without involving external grid absorptions. Both new proposed SC strategies ensure an overall good state of charge at departure time for all the vehicles by distributing the generated PV power as a function of the EV SOC. It means that SC prioritizes charging EVs which present a lower SOC value. On the other hand, in the case of abundant RES availability, the two novels SC strategies ensure optimal exploitation of PV power by allocating the latter as a function

of the vehicle's maximum absorbable power. The main difference between the two optimized charging management systems (OCMSs) lies in the EV power flows direction. The first SC only involves unidirectional power flow; on the other hand, the second one also considers bidirectional power flow among vehicles. Operating in V2V mode, the latter might reduce the charge level of a portion of plugged vehicles in favor of other plugged EVs. The two OCMSs are implemented and tested on an actual case study. Simulations are carried out considering an industrial area having a PV plant, non-modulable electrical loads, and EV charging stations (CS). Results are collected and compared based on uninterrupted power data measurement. Finally, power flows' analysis shows, with an appreciable statistical relevance, the improved performance experienced by operating the novel OCMSs.

The paper is arranged as follows. In *EV Aggregate Charging Demand Evaluation for a Working Place Parking Lot Scenario* Section, the EV aggregate charging demand in the scenario is evaluated. In *SC Method for Self-Consumption Optimization* Section, SC methods are introduced and detailed. Assessment of the results is performed in *Results Discussion* Section. Finally, the conclusion ends the article.

EV AGGREGATE CHARGING DEMAND EVALUATION FOR A WORKING PLACE PARKING LOT SCENARIO

The CMS proposed in this paper aims to control the charging power flows of an aggregated EV population inside the energy district. For the sake of clarity, **Figure 1** shows the structure of a generic PED in which the CMS operates. From the electrical point of view, the reference system consists of the following:

- Electrical loads such as buildings, household consumers, offices, and industrial areas which adsorb a non-modulable power (P_L).
- Internal power sources, usually renewable (RES), such as PV plants that generate an intermittent power (P_{PV}) suppliable to internal loads and the external grid.
- A point of common coupling (PCC) electrically connecting the internal loads and distributed RESs to the external grid. Through the PCC, the grid shares the power P_{PCC} with the PED.
- A population of aggregate EVs connected to the electrical system through the CS. The aggregate EV fleet absorbs the power P_{EVs}. In the case of unidirectional CS (G2V), the EV power is considered positive. In the case of bidirectional power flow, P_{EVs} could assume negative values when V2X operations are carried out.

Following the above convention, the power flow involving the PED can be described through the power balance in **Eq. 1**.

$$P_{PCC}(t) = P_L(t) - P_{PV}(t) + P_{EVs}(t). \qquad (1)$$

From the above equation, it can be noted that even if the internal load and generated power (P_L and P_{PV}, respectively) are not controllable, it is still possible to control external grid
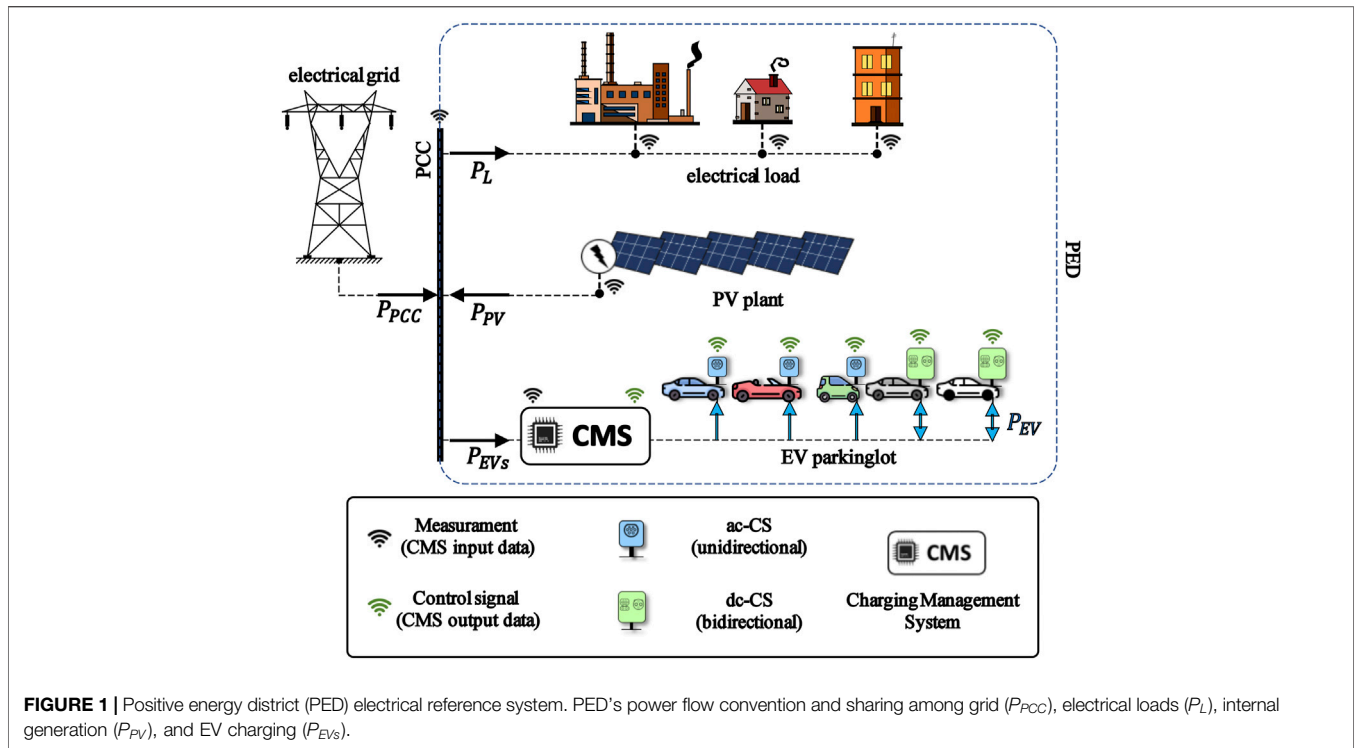
FIGURE 1 | Positive energy district (PED) electrical reference system. PED's power flow convention and sharing among grid (P_{PCC}), electrical loads (P_L), internal generation (P_{PV}), and EV charging (P_{EVs}).

absorptions by managing the aggregate EV power. In this way, the EV population can be considered a controllable and active element of the PED capable of providing power flexibility, optimizing the whole PED consumption, and operating in SC mode. The main task of the proposed SC technique is to increase self-consumption by maximizing EV charging from the PED's internal power source, reducing grid power peaks.

For the implementation of the SC system, both production and load power measurements are necessary. In this paper, the daily load and generation profiles are extracted from yearly acquisitions. The same procedure is done for the PED power-sharing with the grid (PCC measurements). On the other hand, EVs' daily power flow is more challenging to be extrapolated due to its gathering complexity, data lacking, and the statistically weak number of EVs. Current measurement data are not sufficient to extrapolate meaningful EV charging profiles. For these reasons, a predictive method capable of estimating the daily aggregate charging power flows is used and described in *EV Charging Power Flow Calculation Method* Section. Then, in *Reference Scenario and Standard G2V EV Charging Effects on Power Demand* section, the standard G2V charging effects on the power flow of an actual reference scenario are quantitatively evaluated.

EV Charging Power Flow Calculation Method

The aggregate EV power is obtained by collecting the contribution of each i-th vehicle EV_i of the energy district. Defining N_{ch} as the number of vehicles in charging at the

instant t and $P_{EVi}(t)$ as the corresponding charging power of EV_i, the aggregate charging power is given by **Eq. 2**.

$$P_{EVs}(t) = \sum_{i=1}^{N_{ch}} P_{EVi}(t). \tag{2}$$

The charging power P_{EVi} depends on several distinct factors, such as users' behavior, CS power rating, and EV model's specifications. The main factors considered by the predictive method for computing the daily charging power flow are as follows:

- The maximum power made available by the CS, named P_{CSi} (kW), where EV_i is plugged.
- The maximum power P_{EVmaxi} (kW) handleable by EV_i battery.
- The maximum storable energy, which depends on the EV_i maximum battery capacity C_{maxi} (kWh).
- The EV_i SOC at the initial charging instant (SOC_{0i}).
- The parking duration (T_{pki}) defined as the difference between the EV_i departure t_{depi} and arrival t_{arri} times.

To implement the power flows forecasting, the method described in (Lo Franco et al., 2020) has been utilized for carrying out the statistical analysis of vehicles' data and drivers' behavior. Considerations about the CS power rating are obtained from data analysis reported in (European Alternative Fuel Observatory - EAFO, 2021). With reference to the Italian scenario, most of the public charging points (about 90%) have a power rating below 22 kW (standard

EV model	EV share (%)	Battery capacity (kWh)	Specific consumption (kWh/100 km)	Max AC charging (kW)	Max DC charging (kW)
Renault Zoe	22.3	44.1	17.5	22	46
Smart 42	15.4	17.6	16.1	4.6	—
Tesla M3	13.7	50	14.9	11	170
VW up!	11.6	36.8	14.5	7.4	40
Fiat 500	8.9	42	17	11	85
Peugeot 208	7.1	50	16.4	7.4	99
Hyundai Kona	6.0	39	15	11	50
Opel Corsa	5.3	50	17	7.4	99
Nissan Leaf	5.1	40	17.1	6.6	50
Renault Twingo	4.8	23	16.3	22	—

charge), and the latter turns out to be the most widespread value. Thus, in this paper, a homogeneous population of CS, with $P_{CS} = 22$ kW, is considered. The EV population parameters, such as battery capacity, maximum charging power, specific energy consumption C_{SP} (kWh/100 km), and the vehicle models share, are obtained from (UNRAE, 2020; EV Database, 2021). **Table 1** shows the characteristics of the EV population case study employed in this paper. The population coincides with the newly registered EV fleet in Italy during 2020. The data refers to the top 10 best sellers' models. The specific consumption is estimated considering the world harmonized light-duty vehicles test procedure (WLTP). The maximum AC charging power refers to the onboard converter rating, while the maximum DC charging considers the maximum power that the vehicle battery can receive from off-board CS.

As shown in **Table 1**, the charging power strongly differs as a function of the vehicle charging rating in the considered CS and EV population. Regardless of whether AC or DC charging is considered, the power that EV_i absorbs (P_{EVi}) is given by **Eq. 3**.

$$P_{EVi}(t) = \min[P_{CSi}, P_{EVmaxi}(t)]. \tag{3}$$

While P_{CSi} is assumed constant during the entire process, $P_{EVmaxi}(t)$ (that depends on vehicle specification) can decrease during charging. The power flow forecasting algorithm considers the standardized charging protocol (CC-CV) for lithium batteries. A constant current (CC) is provided to the batteries until the voltage reaches the upper-limit value (cut-off voltage). During this phase, the charging power slightly rises following the battery voltage profile. Then a constant voltage (CV) phase begins, and the battery charging current (and power) decreases. The higher the charging rate (C-rate), the more pronounced the CV phase and the lower the SOC value corresponding to the cut-off voltage. Thus, different C-rates may provide different charging profiles. The proposed method considers this phenomenon and emulates the power reduction during the CV phase based on the SOC and the C-rate value. More details about the employed CC-CV charging emulator are presented in (Lo Franco et al., 2020).

The aggregate EV charging demand profile depends on the charging duration of each EV_i. Let be T_{chi} the charging period of the i-th vehicle; it depends on both the parking duration and the
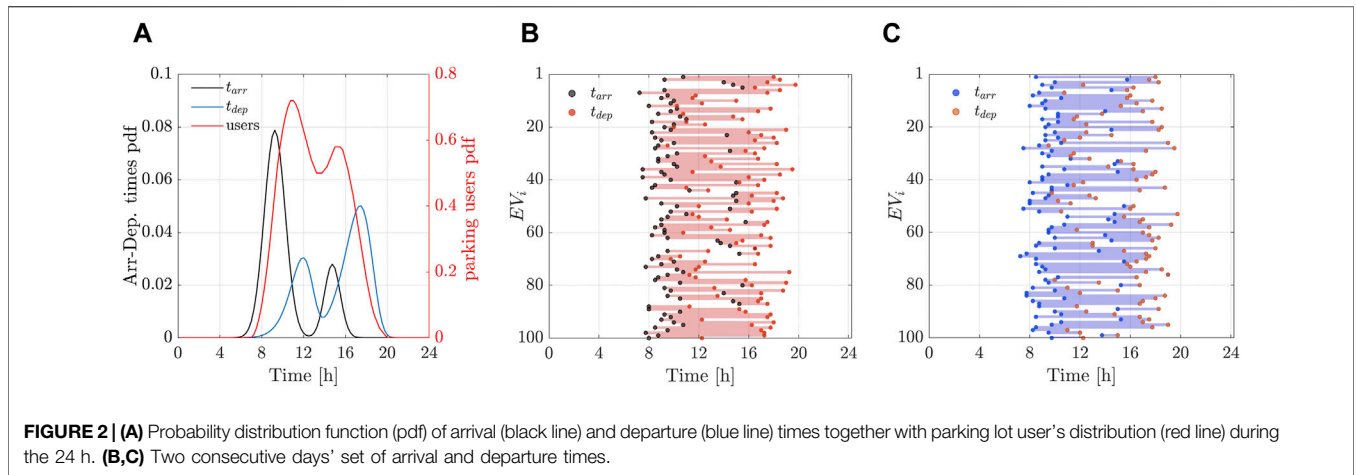
battery SOC evolution during charging ($SOC_i(t)$). The period between charging start (t_{ch0}) and charging end (t_{chf}) is defined as T_{ch}. As shown in **Eq. 4**, it is assumed that t_{ch0} coincides with the arrival time t_{arr}. On the other hand, t_{chf} can whether coincide or not with the instant of departure t_{dep} as reported in **Eq. 5**, depending on the SOC evolution during the charging process. If the vehicle SOC reaches its maximum value (SOC_{max}) before the departure time, the charging period is shorter than the parking duration. On the contrary, T_{ch} coincides with the parking duration if the user leaves the parking lot before full charging. To predict the aggregate daily power flow of an EV population, the parameters in **Eqs 4**, **5** of each EV_i should be calculated.

$$t_{ch0} = t_{arr} \leftrightarrow SOC(t_{ch0}) = SOC_0, \tag{4}$$

$$\begin{cases} t_{chf} < t_{dep} \leftrightarrow SOC(t_{chf}) = SOC_{max} \\ t_{chf} = t_{dep} \leftrightarrow SOC(t_{chf}) < SOC_{max} \end{cases}. \tag{5}$$

Parking times of each EV_i are obtained utilizing statistical analysis of arrival and departure events referring to a working place parking dataset (collected before the COVID-19 global pandemic). **Figure 2** shows the results of the data analysis. **Figure 2A**, left-hand axis, shows the probability distribution function (pdf) of users' arrival (black) and departure (blue) times during the 24 h. On the right-hand axis, the red line shows the parking lot users distribution obtained by the statistical analysis. The values of t_{arri}, t_{depi}, and then the parking duration (T_{pki}) are randomly obtained as a function of the distribution shown in **Figure 2A**. Two sets of t_{arr} and t_{dep} referring to two consecutive days are depicted in the scatter plots of **Figure 2B** and **Figure 2C** that consider a 100-vehicle population. Time T_{pk} of each EV_i is displayed as the band connecting arrival and departure instants. Although arrival and departure times of each i-th vehicle may differ on consecutive days, the overall population's behavior does not change because it is generated from the same distributions (**Figure 2A**).

For all the vehicles, the same value of $SOC_{max} = 90\%$ is assumed. On the other hand, the arrival state of charge (SOC_{0i}) may be different for each vehicle. It depends on the users' behavior (such as the daily traveled distance, D(km)) and

FIGURE 2 | (A) Probability distribution function (pdf) of arrival (black line) and departure (blue line) times together with parking lot user's distribution (red line) during the 24 h. **(B,C)** Two consecutive days' set of arrival and departure times.

the vehicle model characteristics (C_{SPi}; C_{maxi}). The energy $E_{Ci}(d_k)$ (kWh) consumed during a generic day d_k by EV_i is computed from **Eq. 6**.

$$E_{Ci}(d_k) = D_i(d_k)\frac{C_{SPi}}{100} \qquad (6)$$

Based on the statistical analysis carried out in (Lo Franco et al., 2020), a Weibull function having $K = 1.7$ and $\lambda = 37.5$ is used for modeling the daily traveled distance. A similar statistical approach has been discussed in (Ul-Haq et al., 2018; Bernards et al., 2020; Branco and Affonso, 2020). **Figure 3A** shows the distribution of the distance $D(d_k)$ considering a population of 100-vehicles, estimated on seven different days. Introducing the specific consumption and the daily distance traveled by each vehicle in **Eq. 6**, it is possible to calculate the energy consumed by the i-th vehicle on the k-th day. The average daily consumption of the EV population, which is calculated considering the distance $D_i(d_k)$ of **Figure 3A,** is about 5.5 kWh per day.
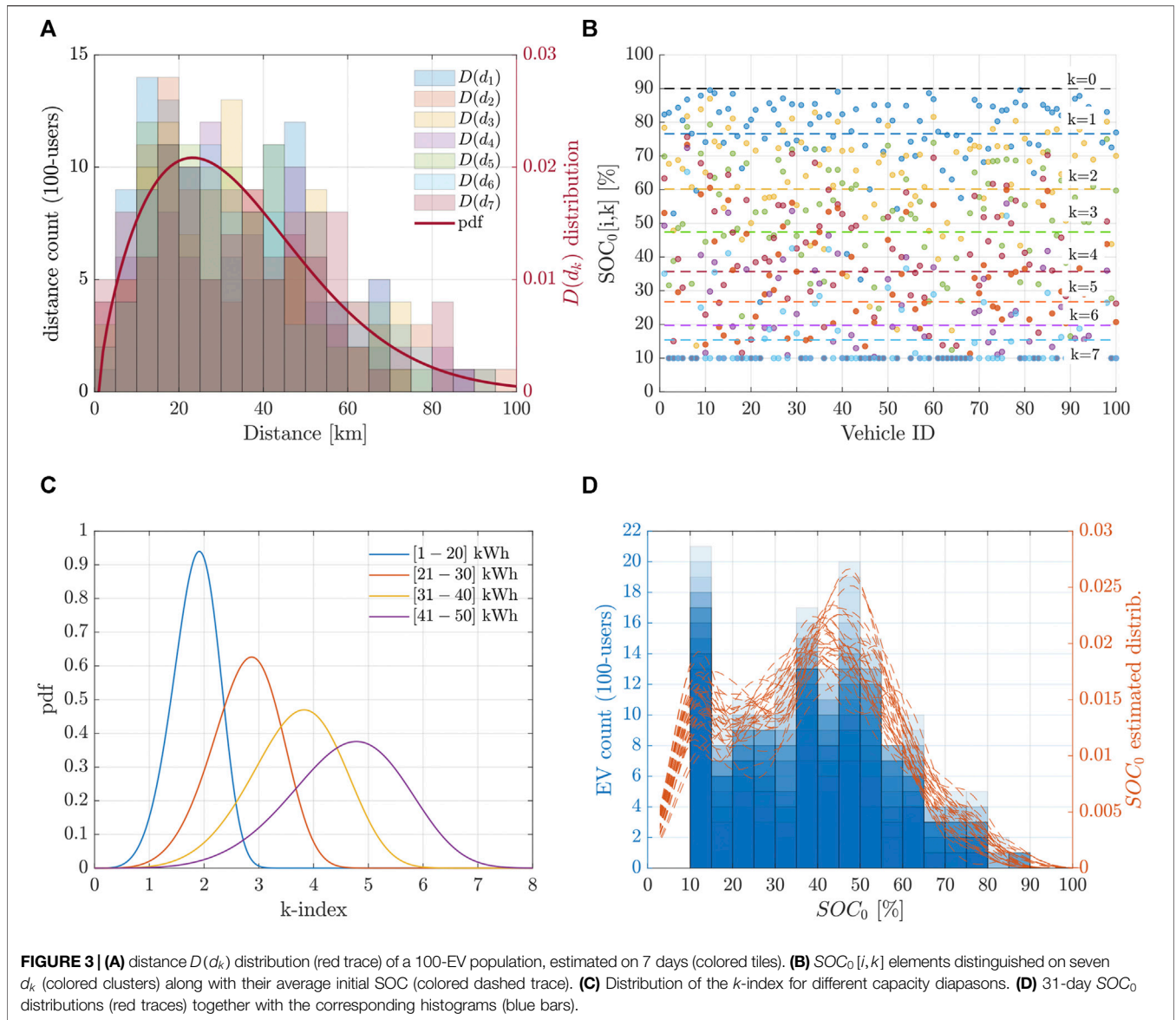
$$SOC_{0i}(d_k) = SOC_i(d_0) - 100\sum_{j=0}^{k-1}\frac{E_{Ci}(d_j)}{C_{maxi}}. \qquad (7)$$

To calculate the $SOC_{0i}(d_k)$ (initial SOC of the i-th EV at the k-th day), **Eq. 7** is used. The first term of **Eq. 7** represents the maximum initial SOC ($SOC_i(d_0) = SOC_{max}$) occurring at day d_0 after the last complete total charge, while $\sum_{j=0}^{k-1}E_{Ci}(d_j)$ is the cumulative energy consumption experienced during the k days before the d_k day. For example, $SOC_{0i}(d_3)$ considers the consumption of the previous 3 days (starting from the last full charging), namely, $E_{Ci}(d_0)$, $E_{Ci}(d_1)$, and $E_{Ci}(d_2)$. **Equation 7** dependence from i- and k-indexes can be generalized over a matrix $SOC_0[i,k]$ having i-row and k-column referring to the i-th EV and d_k, respectively. The scatter plot of **Figure 3B** shows the $SOC_0[i,k]$ elements. For each EV_i, seven d_k are considered (colored clusters). Colored dashed lines represent the average initial SOC at the k-th day. Having assumed $k = 7$ as the maximum value, it is equivalent stating that the extreme case corresponds to a charge once a week (in other words, the seventh column of $SOC_0[i,k]$ contains the

arrival SOC values considering a charging which takes place once a week for each EV_i).

The energy consumption during the days after the last full charging (d_0) must consider EV_i battery capacity. Moreover, together with the SOC_{max} upper constraint, it is assumed $SOC_{min} = 10\%$, reducing the suitable capacity to 80% of C_{max}. Making reference to four capacity diapasons of **Figure 3C**, the maximum suitable capacities are 16 kWh, 24 kWh, 32 kWh, and 40 kWh (in ascending order). Therefore, inequality $\sum_{j=0}^{k-1} E_{Ci}(d_j) \leq 0.8\, C_{maxi}$ holds for each EV_i. This hypothesis affects the maximum number of days that might possibly pass since the last full charge as a function of C_{maxi}. Considering an average daily consumption of 5.5 kWh, the maximum values of k that can be considered for the $SOC_0(d_k)$ evaluation are 3, 4, 6, and 7 for C_{max} ranges (1–20 kWh), (21–30 kWh). (31–40 kWh), and (41–50 kWh), respectively (**Figure 3C**). Finally, the SOC_0 population is obtained by randomly collecting $SOC_0[i,k]$ values, where each k-index is selected employing the Weibull functions of **Figure 3C**. As visible, four capacity diapasons are considered up to $C_{max} = 50$ kWh, which is the higher capacity value of the examined EV population (**Table 1**). Employing the previous hypotheses and the above-described method, the arrival SOC of the EV population is obtained considering in detail the users' behavior and vehicle characteristics. **Figure 3D** shows the estimated distribution of SOC_0 population (red curve, right-hand axis) considering the 31-day set (1-month estimation). On the other hand, the histogram shows the vehicle count using a 5% bin width of SOC. Although the 31-day set of SOC_0 distribution shown in **Figure 3D** varies every day, the overall trend fairly approximates the logic used for the random generation.

Finally, information about each EV's parking time and arrival SOC and data in **Table 1** are used as input in a dynamic model developed in MATLAB/Simulink (MathWorks) environments. The model calculates the charging power profile of each EV_i with a 1 min resolution (**Eq. 3**) and for each time step resolves **Eq. 2** providing as output the aggregate charging demand profile of the examined EV fleet. More details on the predictive EV power flow model have been already presented in (Lo Franco et al., 2020).
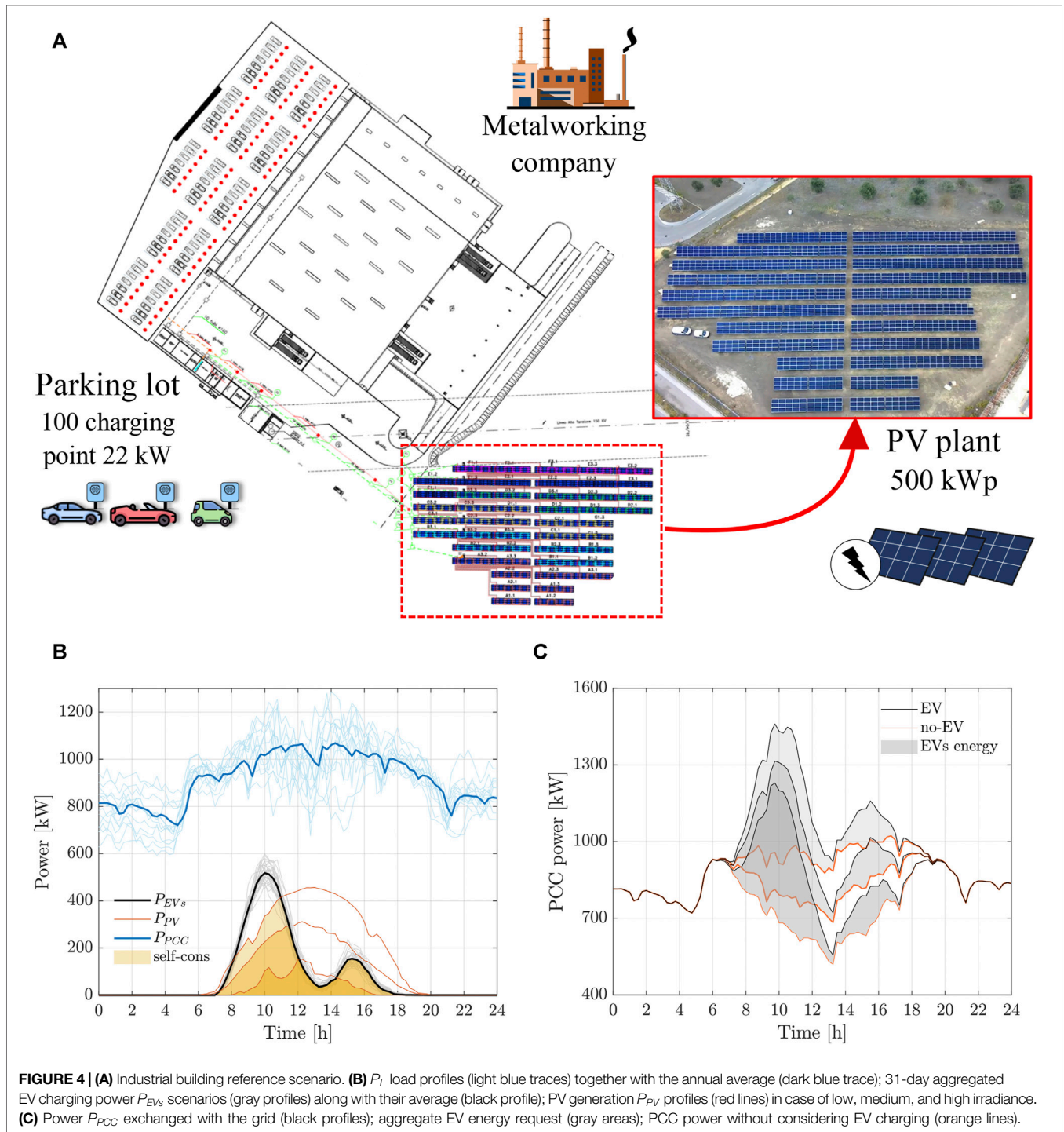
FIGURE 3 | (A) distance $D(d_k)$ distribution (red trace) of a 100-EV population, estimated on 7 days (colored tiles). **(B)** $SOC_0[i,k]$ elements distinguished on seven d_k (colored clusters) along with their average initial SOC (colored dashed trace). **(C)** Distribution of the k-index for different capacity diapasons. **(D)** 31-day SOC_0 distributions (red traces) together with the corresponding histograms (blue bars).

The following section will show the predictive EV charging model results and the EV charging demand effects on an actual case study.

Reference Scenario and Standard G2V EV Charging Effects on Power Demand

Figure 4A shows the reference scenario employed in the simulation. It represents an industrial building (metalworking company) with 50% EV penetration represented by a parking lot of 100 stands having 22 kW charging ports each. The internal generation is provided by a 500 kWp PV plant. Aggregated EV load is calculated, and its impact on the daily plant power profile is evaluated. The metalworking company load $P_L(t)$ and the PV power flows $P_{PV}(t)$ as a function of time are obtained by uninterrupted measurements over a period of 1 year (24/7/365 power data measurement). More details about data are reported

in (Lo Franco et al., 2020). In **Figure 4B**, some P_L load profiles (light blue traces) together with the annual average (dark blue trace) are depicted. Furthermore, 31-day aggregated EV charging power P_{EVs} scenarios (gray profiles) along with their average (black profile) are reported. The scenarios are obtained starting from the set of 31 SOC_0 of **Figure 3B** and the t_{arr}/t_{dep} visible in **Figure 2**. Finally, three PV generation P_{PV} profiles (for highlighting the RES discontinuity) are reported as well (red lines). The latter represents low irradiance (where the daily PV-generated energy is 588 kWh/d), medium irradiance (2090 kWh/d, average of 1-year data), and high irradiance (3,527 kWh/d) scenarios. Orange-filled areas represent the self-consumption energy share provided to EVs from the internal PV source in the three irradiance conditions. Introducing these power profiles in **Eq. 1**, it is possible to calculate the power P_{PCC} exchanged with the grid shown in **Figure 4C**. The black traces consider average P_L and P_{EVs}

FIGURE 4 | (A) Industrial building reference scenario. **(B)** P_L load profiles (light blue traces) together with the annual average (dark blue trace); 31-day aggregated EV charging power P_{EVs} scenarios (gray profiles) along with their average (black profile); PV generation P_{PV} profiles (red lines) in case of low, medium, and high irradiance. **(C)** Power P_{PCC} exchanged with the grid (black profiles); aggregate EV energy request (gray areas); PCC power without considering EV charging (orange lines).
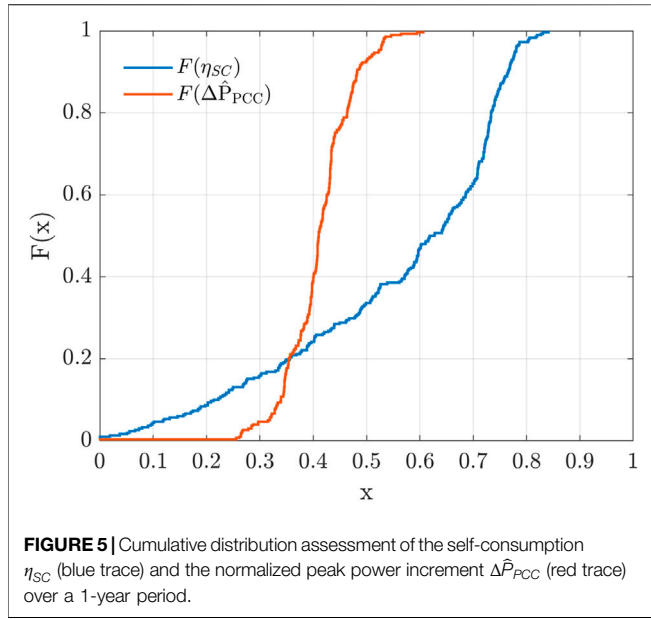
together with the three P_{PV} cases. The orange lines depict the net power drawn from the grid without considering EV charging. Finally, gray areas represent the additional charging energy required to the grid by the EV fleet.

To quantitatively characterize the effects of aggregate EV charging on power flow and evaluate EV profile overlapping with the PV generation, some figures of merit are defined. The ratio between the orange area of **Figure 4B** and the total EV

charging energy (gray area in **Figure 4C**)) is the charging self-consumption coefficient η_{SC}. η_{SC} is 1 if the internal generation manages to fully provide the energy required by the EV charging. On the other hand, η_{SC} is 0 if the charging energy is entirely drawn from the grid (external power source).

To evaluate the effect of EVs charging on PCC power flow, the normalized peak power $\widehat{P}_{PCC}$, defined in **Eq. 8**, is considered, which quantifies the maximum daily peak load with respect to the

FIGURE 5 | Cumulative distribution assessment of the self-consumption η_{SC} (blue trace) and the normalized peak power increment $\Delta \hat{P}_{PCC}$ (red trace) over a 1-year period.

average daily load without considering the EV charging. This indicator can be calculated also considering the maximum PCC power in the case of EV charging ($\hat{P}_{PCC}^{EV}$).

$$
\begin{cases}
\hat{P}_{PCC} = \dfrac{\max(P_{PCC}) - <P_{PCC}>}{<P_{PCC}>} \\[3mm]
\hat{P}_{PCC}^{EV} = \dfrac{\max(P_{PCC}^{EV}) - <P_{PCC}>}{<P_{PCC}>}
\end{cases}
\rightarrow \; \Delta\hat{P}_{PCC} = \hat{P}_{PCC}^{EV} - \hat{P}_{PCC}
$$

$$(8)$$

The annual analysis carried out for evaluating η_{SC} and $\Delta\hat{P}_{PCC}$ considering the seasonal and daily variability of both PV generation and PCC load is depicted in **Figure 5**. The cumulative distribution of η_{SC} (blue trace) shows that the maximum value of charging self-consumption is about 0.85 (100% of simulated days presents η_{SC} < 0.85) while the average value is 0.55. Moreover, **Figure 5** shows the cumulative distribution of $\Delta\hat{P}_{PCC}$. Considering the reference scenario, it is shown that aggregate EV charging increases the peak power up to 60% in comparison with the no-EVs scenario (under worst conditions), while practically all the simulated days show an increase of more than 20%. The $\Delta\hat{P}_{PCC}$ average increment is of about 40%.

To improve the EV aggregate charging impact on power flows (mitigate $\hat{P}_{PCC}^{EV}$ increment) and maximize charging from internal PV (increase η_{SC}), a novel CMS capable of operating in SC is developed and applied to the reference scenario's power flows.

SC METHOD FOR SELF-CONSUMPTION OPTIMIZATION

To improve performances, increase charging self-consumption, and mitigate the detrimental effects due to grid power peaks, a CMS has been proposed in (Lo Franco

et al., 2020). This CMS permits the management of the charging power of each EV leading to SC mode operations. It aims to optimize η_{SC} meantime reducing PCC peak power increment $\Delta\hat{P}_{PCC}$. This optimization is achieved by actively changing the maximum CS power (for instance, acting on the control pilot pin of Type-2 plugs (IEC 62196-1 TC 23/SC 23H, 2014)).

Considering a 1-day simulation, the charging self-consumption is defined by

$$
\eta_{SC} = \dfrac{\int_0^{24} \min(P_{PV},\, P_{EVs})\, dt}{\int_0^{24} P_{EVs}\, dt}.
$$

$$(9)$$

The proposed management system operates with a 1 min sampling. In each time step, it is possible to assume constant P_{PV} and P_{EVs}. Then, the charging self-consumption in each 1 min time step (η_{SCm}) is obtained by

$$
\eta_{SCm} = \dfrac{\min(P_{PV},\, P_{EVs})}{P_{EVs}}.
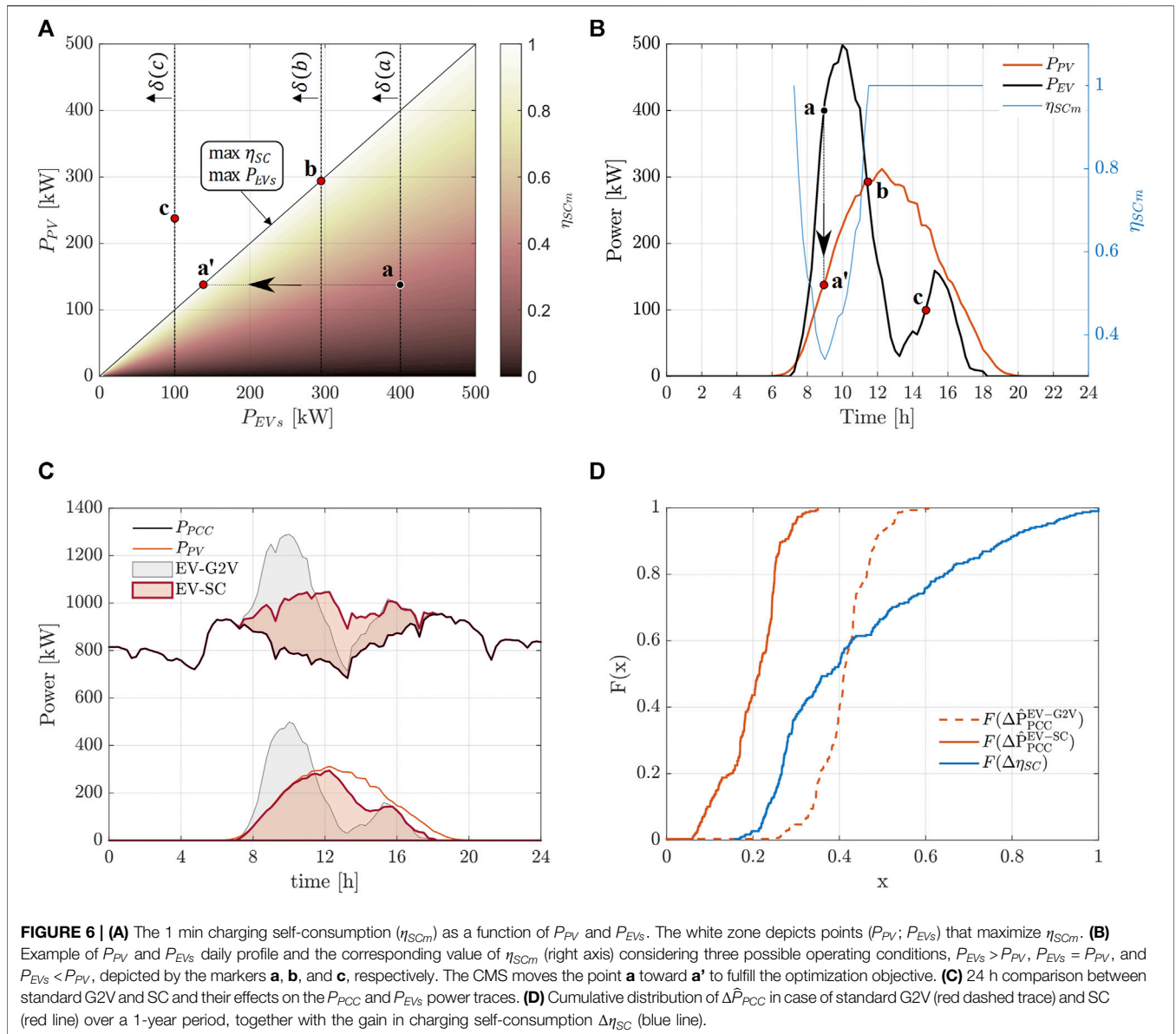$$

$$(10)$$

Considering the PV power availability and the EV power demand at a generic instant t, the main target of the proposed SC methods is to manage the aggregate EV charging to maximize $\eta_{SCm}(t)$ providing the maximum value of P_{EVs}. The optimization objective can be summarized by **Eq. 11**.

$$
\text{objective:} \begin{cases} \max \eta_{SCm} \\ \max P_{EVs} \end{cases},
$$

$$(11)$$

$$
\text{constraints:}\; 0 \le P_{EVS} \le \sum_{i=1}^{N_{ch}} P_{EVimax},
$$

$$(12)$$

where the problem's constraints are reported in **Eq. 12**. The constraint equation is given by **Eq. 3** and depends on the vehicle's model, the number of plugged vehicles, and the SOC level evolution during the charging process (please refer to EV *Aggregate Charging Demand Evaluation for a Working Place Parking Lot Scenario* Section of the paper for more details). Moreover, the constraint ensures the unidirectionality of power flows.

The solution can be obtained considering **Figure 6A** that shows the contour plot of η_{SCm} as a function of P_{EVs} and P_{PV}. The color bar shows the value of η_{SCm}. The white color in the figure depicts points with $\eta_{SCm} = 1$; on the other hand, the colored area depicts points (P_{EVs}; P_{PV}) having η_{SCm} < 1. **Figure 6B** shows, as an example, the PV and EVs charging power profile (left axis) during a typical day and the corresponding value of η_{SCm} (right blue axis). Three possible operating conditions are pointed out in the figure: $P_{EVs} > P_{PV}$, $P_{EVs} = P_{PV}$, and $P_{EVs} < P_{PV}$, depicted by the markers **a**, **b**, and **c**, respectively. The three examined operating conditions are also marked in **Figure 6A**, where the dotted line represents the boundaries, $\delta(a)$, $\delta(b)$, and $\delta(c)$, of the admissible solutions obtained by the constraints of **Eq. 12**. The point **b** and **c** fulfill both the optimization objectives and constraints of **Eqs 11**, **12**, respectively. On the other hand, point **a** is not an optimal working point. In this case, the CMS reduces the aggregate P_{EVs} to overlap the PV availability by

FIGURE 6 | (A) The 1 min charging self-consumption (η_{SCm}) as a function of P_{PV} and P_{EVs}. The white zone depicts points (P_{PV}; P_{EVs}) that maximize η_{SCm}. **(B)** Example of P_{PV} and P_{EVs} daily profile and the corresponding value of η_{SCm} (right axis) considering three possible operating conditions, $P_{EVs} > P_{PV}$, $P_{EVs} = P_{PV}$, and $P_{EVs} < P_{PV}$, depicted by the markers **a**, **b**, and **c**, respectively. The CMS moves the point **a** toward **a'** to fulfill the optimization objective. **(C)** 24 h comparison between standard G2V and SC and their effects on the P_{PCC} and P_{EVs} power traces. **(D)** Cumulative distribution of $\Delta\hat{P}_{PCC}$ in case of standard G2V (red dashed trace) and SC (red line) over a 1-year period, together with the gain in charging self-consumption $\Delta\eta_{SC}$ (blue line).

shifting the point **a** toward **a'**, which is the optimal point at the examined irradiance conditions.

Finally, it is possible to note that the points that fulfill **Eq. 11** are represented by the diagonal black line ($P_{EVs} = P_{PV}$) in **Figure 6A**. Since P_{EVs} is the sum of each P_{EVi} as shown in **Eq. 2** of *EV Aggregate Charging Demand Evaluation for a Working Place Parking Lot Scenario* Section, the CMS computes the reference charging power P_{EVi}^* for the CS having plugged the i-th EV as in **Eq. 13** to ensure the optimal operating condition. The internal generation power P_{PV} is therefore evenly shared among the N_{ch} plugged EVs.

$$P_{EVi}^*(t) = \frac{P_{PV}(t)}{N_{ch}(t)}. \tag{13}$$

Through **Eq. 13**, the CMS modulates each vehicle charging to ensure that the aggregate charging power overlaps the PV available power ($\sum P_{EVi}^* = P_{EVs} = P_{PV}$) complying with **Eq. 11** and constraints of **Eq. 12**. In other words, based on the PV availability and the plugged EVs' power demand, the CMS moves the working point from the colored zone of **Figure 6A**, toward the diagonal line (optimal operation) by acting on each EV charging power. As a result, the charging self-consumption increases, and the SC minimizes the absorption of energy from the grid favoring the charging from the internal PV source. **Figure 6C** shows the effects of SC on power flows. EV-related power shifts from gray shaded distribution labeled "EV-G2V" (already depicted in **Figure 4**) toward the red shaded labeled as "EV-SC." **Figure 6D** compares the charging performance in terms of peak power and η_{SC} between SC and standard (G2V) charging

TABLE 2 | Quantitative comparison between standard G2V charging and SC performance under low (588 kWh/d), medium (2090 kWh/d), and high (3,527 kWh/d) irradiance PV scenarios.

PV energy (kWh]	Standard (G2V)			Smart charging (CMS)		
	η_{SC}	$\hat{P}_{PCC}$	EVs energy (kWh)	η_{SC}	$\hat{P}_{PCC}$	EVs energy (kWh)
588	0.27	0.51		1	0.16	587
2090	0.68	0.45	1856	1	0.17	1609
3527	0.85	0.42		1	0.21	1745

(as in **Figure 5**) over a 1-year period. The cumulative distribution $\Delta\hat{P}_{PCC}^{EV-SC}$ when SC is considered (red line) settles around a 20% average value (20% more than the no-EV scenario). On average, $\Delta\hat{P}_{PCC}$ experienced under SC is about half of the one under uncontrolled G2V, labeled $\Delta\hat{P}_{PCC}^{EV-G2V}$ (red dotted line) in **Figure 6D**. The proposed SC ensures to always experience self-consumption coefficient η_{SC} equal to 1. The blue line in **Figure 6B** depicts the cumulative distribution over 1-year results of the charging self-consumption increment ($\Delta\eta_{SC}$) experienced operating in SC with respect to standard G2V charging. Results show $\Delta\eta_{SC}$ average value of about +45%. Moreover, **Table 2** collects a quantitative comparison between standard G2V charging and SC performance under low (588 kWh/d), medium (2,090 kWh/d), and high (3,527 kWh/d) irradiance PV scenarios.

Although the results show an improvement in charging self-consumption and a reduction in PCC peak power, the above-described SC method presents two relevant weaknesses:

- **Weakness 1.** The CMS based on **Eq. 13** provides less total energy to the vehicles compared to standard G2V charging. Indeed, E_{EVs}^{SC} is generally lower than E_{EVs}^{G2V}. The higher the available PV power, the lower the energy mismatch. For instance, referring to **Table 2**, under mean values of irradiance (2,090 kWh/day), the charging self-consumption increases up to +32%, the difference in peak power is about −28%, and the charging energy deficit is about 13%. Moreover, in the case of high irradiance (3,527 kWh/day), the energy deficit decreases up to only 5%. Although η_{SC} and ΔP_{PCC} improve, the trade-off between self-consumption and EV charging energy is not satisfactory in case of low irradiance. Consequently, EVs' SOC at the instant of departure is particularly low compared to the standard charging counterpart because the CMS is charging the EV population using only the internal generation (which is lower than the EV request).
- **Weakness 2.** Under the condition where the power required by the whole EV fleet is totally covered by PV generation, the charging may still underutilize the available PV energy. Since the CMS based on **Eq. 13** equally allocates P_{PV} to the plugged EVs, if the assigned reference power, P_{EVi}^*, is higher than P_{maxi}, a curtailment power phenomenon caused by the maximum charging power bottleneck takes place. Thus,

even if $\sum P_{EVi}^* = P_{PV}$, the actual P_{EVs} may be lower leading to $\sum P_{EVi} < P_{PV}$.

A suboptimal solution could be to charge the vehicles from the grid during low irradiance availability, nevertheless leading to a self-consumption reduction of the whole district. Two novel charging strategies are investigated to verify which improvements could be achieved by handling differently the EVs charging without involving the external grid (no detrimental effect on η_{SC} and load flattening capability). Although both CMS algorithms aim to overcome previously described drawbacks, they differ by the ability to have either unidirectional (SC) or bidirectional (V2V) operations. The proposed solutions are as follows:

- **Solution 1.** Instead of evenly share P_{PV} among the connected vehicles, a smart allocation of the energy to support the charging of vehicles with a lower SOC level rather than those with a higher SOC (or that recharge faster) can be used. The target of the novel OCMS is to improve EV SOC level allocation by decreasing its standard deviation among the fleet. In other words, prioritize EVs having low SOC_i guaranteeing an overall good SOC level at departure time for all the vehicles. In addition to **Eq. 11**, the OCMS aims to fulfill the objective of **Eq. 14**, where $\overline{SOC}$ is the average SOC of the plugged EV population.

$$\min \sum_{i=1}^{N_{ch}} \left| SOC_i - \overline{SOC} \right|. \tag{14}$$

- **Solution 2.** To overcome weakness 2, which occurs when the PV power is more or equal to the aggregate EV power request, the OCMS allocates each P_{EVi}^* as a function of the maximum power that the EV_i's battery can adsorb. In this way, the whole available PV power is used for charging, avoiding the bottleneck phenomenon of the maximum charger rating. In addition to **Eqs 11**, **14**, the OCMS aims to also fulfill the objective of **Eq. 15**.

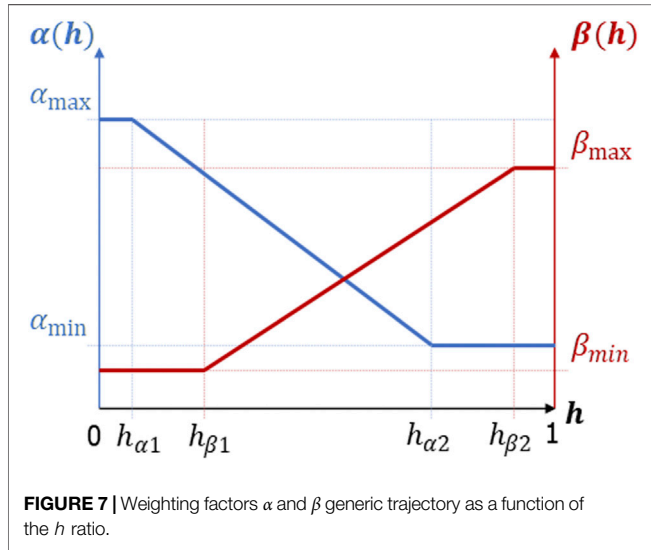$$\min \sum_{i=1}^{N_{ch}} \left| P_{EVi} - P_{EVmaxi} \right|. \tag{15}$$

Although they both overcome the above weaknesses, the two proposed OCMS differ for the power flow direction. The first only consider the PV to EV flow and is indicated as unidirectional OCMSs (OCMS) (1d-OCMS). On the other hand, the second one is defined as bidirectional OCMS (2d-OCMS) because it also considers the power flow among EVs (V2V). The main difference is that the 2d-OCMS might reduce the charge level of a portion of plugged vehicles (discharging operation) in favor of other plugged EVs. Finally, **Table 3** summarizes the optimization objective and constraints between the CMS and the proposed novel 1d-OCMS and 2d-OCMS.

Unidirectional OCMS, 1d-OCMS

The unidirectional OCMS, 1d-OCMS, allocates the reference charging power of each EV_i based on **Eq. 16**, as a function of

TABLE 3 | Problem's objectives and constraints of the proposed charging management systems.

Problem	CMS	1d-OCMS	2d-OCMS
Objectives	$\max \eta_{SCm}$	$\max \eta_{SCm}$	$\max \eta_{SCm}$
	$\max P_{EVs}$	$\max P_{EVs}$	$\max P_{EVs}$
	—	$\min \sum_{i=1}^{N_{ch}} |SOC_i - \overline{SOC}|$	$\min \sum_{i=1}^{N_{ch}} |SOC_i - \overline{SOC}|$
	—	$\min \sum_{i=1}^{N_{ch}} |P_{EVi} - P_{EVmaxi}|$	$\min \sum_{i=1}^{N_{ch}} |P_{EVi} - P_{EVmaxi}|$
Constraints	$P_{EVs} \geq 0$	$P_{EVs} \geq 0$	$P_{EVs} \geq 0$
	$P_{EVs} \leq \sum_{i=1}^{N_{ch}} P_{EVimax}$	$P_{EVs} \leq \sum_{i=1}^{N_{ch}} P_{EVimax}$	$P_{EVs} \leq \sum_{i=1}^{N_{ch}} P_{EVimax}$
	$P_{EVi} \geq 0$	$P_{EVi} \geq 0$	—

FIGURE 7 | Weighting factors α and β generic trajectory as a function of the h ratio.

both the vehicle depth of discharge DOD_i (defined as $SOC_{max} - SOC_i$) and the maximum value of the charging power (P_{maxi}).

$$P_{EVi}^* = \frac{DOD_i^\alpha P_{maxi}^\beta}{\sum_{j=1}^{N_{ch}} DOD_j^\alpha P_{maxj}^\beta} P_{PV} = A_i P_{PV}. \quad (16)$$

The exponents α and β are weighting factors that vary as a function of the instantaneous ratio between the PV power availability and the total EV power demand, named h in **Eq. 17**.

$$\begin{cases} h = \dfrac{P_{PV}}{\sum_{j=1}^{N_{ch}} P_{maxj}} = \dfrac{P_{PV}}{P_{maxEVs}} \\ \alpha = \alpha(h) \\ \beta = \beta(h) \end{cases}. \quad (17)$$

Note that h varies because of the daily irradiation P_{PV}, number of connected vehicles N_{ch}, and P_{maxi}. Moreover, P_{maxi} can decrease during the charging process due to the CV phase of the Li-ion battery charging protocol. Then, replacing **Eq. 16** into **Eqs 17** and **18** can be found.

$$P_{EVi}^* = A_i(h) P_{maxEVs} h. \quad (18)$$

Since $\sum_{i=1}^{N_{ch}} A_i = 1$, it is ensured that $\sum_{i=1}^{N_{ch}} P_{EVi}^* = P_{PV}$. By means of coefficient A_i, the available PV power is differently allocated among EVs as a function of h.

Weighting factors α and β generic trajectory as a function of the h ratio are shown in **Figure 7**. Under low irradiance conditions (weaknesses 1), when the EVs' demand is higher than the P_{PV} ($h < 1$), the target is to prioritize EVs having low SOC_i guaranteeing an overall good SOC level at departure time for all the vehicles. For this reason, the proposed strategy increases coefficient α, promoting the SOC-based allocation of A, as h decreases. When h is below the lower threshold $h_{\alpha 1}$ (close to 0), α assumes its very maximum value α_{max}. On the other hand, when h increases and overcome the upper threshold $h_{\alpha 2}$ (close to 1), the SOC-based weighting is no longer necessary as the PV is sufficient to satisfy the EV charging request. Thus, α deepens to its minimum value $\alpha(h_{\alpha 2}) = \alpha_{min}$; therefore, $[h_{\alpha 2}, \alpha_{min}] = [1, 0]$. On the other hand, the β coefficient, which influences the P_{max}-based allocation of A, assumes a complementary trend as h varies. Under medium-high irradiance conditions (weaknesses 2), when h overcomes the upper threshold ($h_{\beta 2} = 1$), $\beta(h_{\beta 2}) = \beta_{max}$. To avoid the EV charging rating bottleneck problem, $[h_{\beta 2}, \beta_{max}] = [1, 1]$. In this way, when $h \geq 1$, $A_i(h \geq 1)$ makes sure that $P_{EVi}^* = P_{maxi}$ for each vehicle undercharging. The tuning of the α and β weighting functions in the point $[h_{\alpha 1}, \alpha_{max}]$ and $[h_{\beta 1}, \beta_{min}]$ is described in *Results and Discussion* section.

Bidirectional OCMS, 2d-OCMS (V2V Operation)

The bidirectional OCMS, 2d-OCMS, allocates the reference charging power of each EV_i based on **Eq. 19**, as a function of both the vehicle SOC_i and the maximum value of the charging power P_{maxi}.

$$P_{EVi}^* = P_{maxi} - \frac{SOC_i P_{maxi}}{\sum_{j=1}^{N_{ch}} SOC_j P_{maxj}} (P_{maxEVs} - P_{PV}). \quad (19)$$

Replacing in **Eq. 17** the weighting factor B_i defined in **Eq. 20**, the dependence of P_{EVi}^* from h can be explicated as in **Eq. 21**. Since $\sum_{i=1}^{N_{ch}} B_i = 1$, it is ensured that $\sum_{i=1}^{N_{ch}} P_{EVi}^* = P_{PV}$.

$$B_i = \frac{SOC_i P_{maxi}}{\sum_{j=1}^{N_{ch}} SOC_j P_{maxj}}, \quad (20)$$

$$P_{EVi}^* = P_{maxi} - B_i P_{maxEVs}(1 - h). \quad (21)$$

If the PV availability is sufficient to guarantee the maximum charging power for all plugged vehicles ($h \geq 1$), the reference power P^*_{EVi} coincides with P_{maxi} solving weakness 2. Since P_{max} is the EV's maximum absorbable power, if $h > 1$, the surplus of PV power is provided to other loads or injected into the grid. On the other hand, when $h < 1$, P^*_{EVi} decreases with respect to its maximum value by a factor proportional to h and to the value of SOC_i and P_{maxi}. In this way the 2d-OCMSs differently allocate power among vehicles, supporting the charging of vehicles with a lower SOC level rather than those with a higher SOC, solving weakness 1. Moreover, in case some vehicles have a similar SOC value, the B_i coefficient prioritizes EVs with a faster charging capability.

The difference with respect to the 1d-OCMS is that the P^*_{EVi} assigned by the 2d-OCMS may assume a negative value. This phenomenon happens when the variance among vehicles' SOC is high, and the PV power availability is low. **Equation 22** shows the value of h which provides negative charging powers (discharging phase).

$$P^*_{EVi} < 0 \leftrightarrow h < 1 - \frac{P_{maxi}}{B_i \, P_{maxEVs}}. \quad (22)$$

During the discharging phase, EVs which have higher SOC share a fraction of their energy with vehicles having lower SOC levels. The discharging power remains proportional to B_i and within the maximum limits allowed by the charging infrastructure. This smart charging-discharging operating among EVs can be classified as vehicle-to-vehicle (V2V) mode.

Unlike the unidirectional power flow, which only considers the direction from an energy source X to the EV (X2V), the bidirectional power flow, which contemplates EV's battery discharging toward a generic load (V2X), is feasible only if the charging infrastructure allows it. At the current stage, it is not possible to invert the power flows with AC-CS since the charging parameters (voltages and currents) are mainly managed by the vehicle onboard converter. Furthermore, the communication protocols between the AC-CS and the EV (PWM/impedance modulation in control pilot pin of the Type 2 connector (IEC 62196-1 TC 23/SC 23H, 2014)), despite allowing charging power modulation, does not permit power flow inversion. For these reasons, the V2V (in general V2X) mode may currently be feasible only via DC-CSs (off-board charging), which, as **Table 1** shows, bypasses the onboard converter size limitation providing higher-rated powers. However, in order to compare the performance of the different proposed CMSs, this paper assumes the same charging rating for each EV, both considering AC or DC charging.
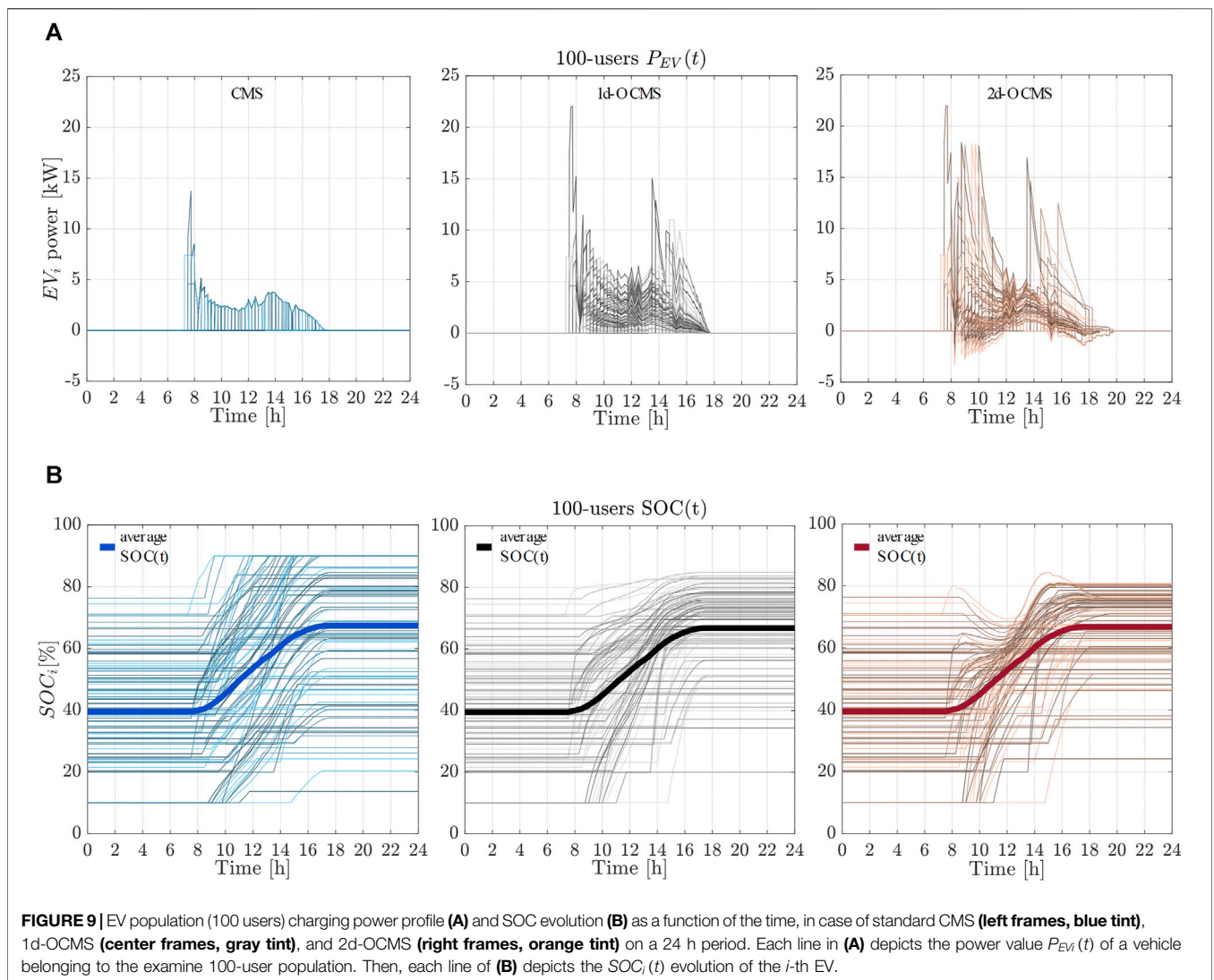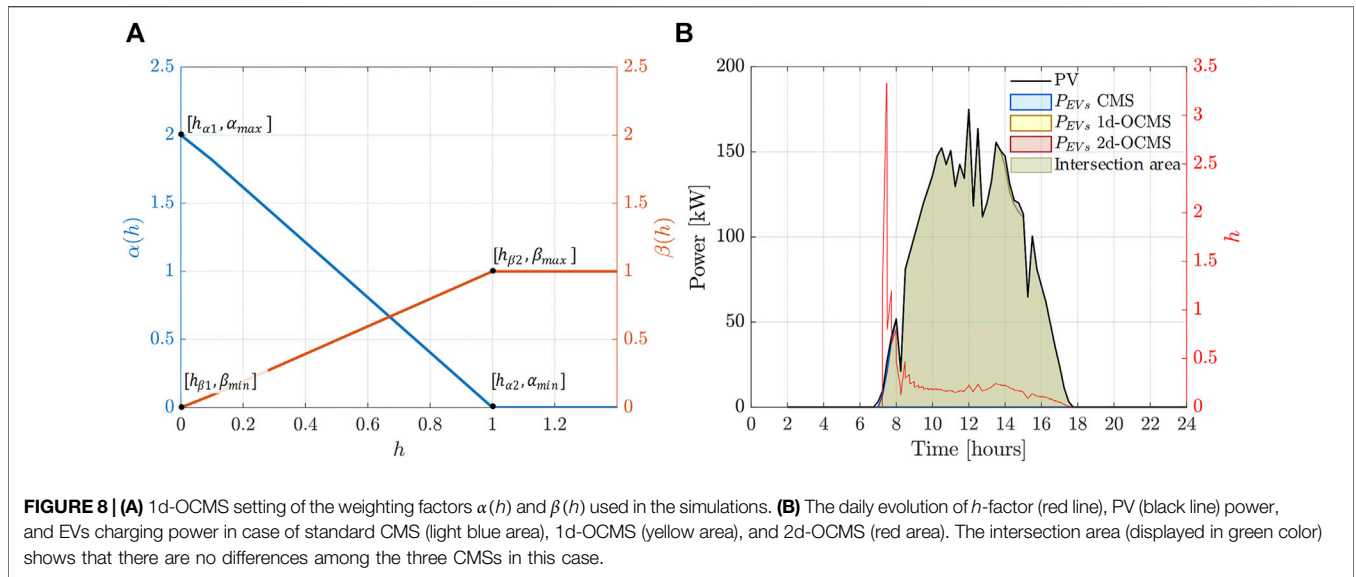
RESULTS AND DISCUSSION

This section shows and discusses the obtained results considering applying the two novel OCMSs on the reference scenario described in *Reference Scenario and Standard G2V EV Charging Effects on Power Demand* section. Simulations are carried out using MATLAB/
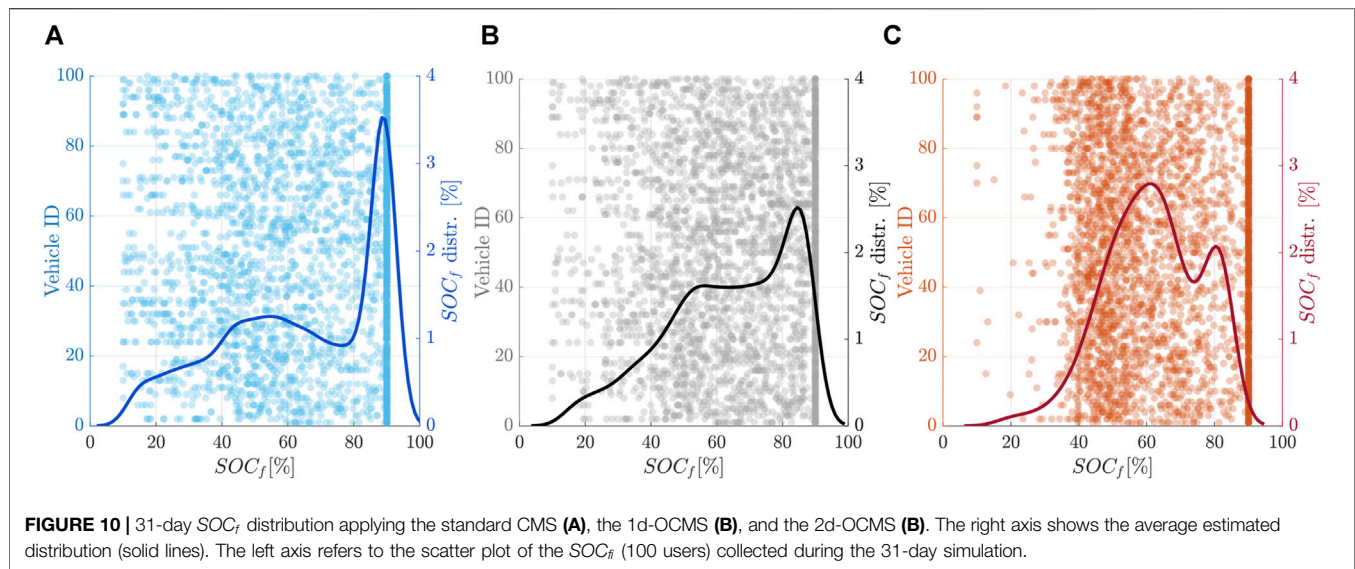
Simulink. A comparison between 1d-OCMS, 2d-OCMS, and the standard CMS is carried out in terms of EV fleet-level charging performance improvement. Since both OCMSs aim to mitigate the above weaknesses which happen under specific conditions, both techniques are simulated considering low irradiance conditions (low h ratio value) and high irradiance scenario (h ratio around 1 or more) referring to weaknesses 1 and 2, respectively. Together with them, standard CMS described in **Eq. 13** is reported as well.

To better understand how the standard and the proposed standard CMS and the two proposed OCMS operate, simulations were run considering a winter-day (medium-low irradiance scenario). The effects on power flows of the different SC algorithms are displayed in **Figure 8** and **Figure 9**. From multivariate analysis on 1d-OCMS performance, the best results were achieved calling off the β coefficient weight when $h = 0$. On the other hand, the α-coefficient weight is kept higher than one around $h = 0$ to enhance the SOC-based allocation of A under low irradiance conditions. However, $\alpha_{max} > 2$ provides a detrimental effect on the total EV charging energy. In fact, although **Eq. 16** tries to allocate the whole PV power, high values of α_{max} might cause on certain EV_i (especially those with lower SOC) an allocation of the reference power P^*_{EVi} higher than what they can accept. In this way, the curtailment power phenomenon caused by the maximum charging power bottleneck (weakness 2) may also appear with a low value of h. For these reasons, the last points which define the weighting parameters as a function of h are $[h_{\alpha 1}, \alpha_{max}] = [0, 2]$ and $[h_{\beta 1}, \beta_{min}] = [0, 0]$. **Figure 8A** shows the final setting of the weighting factors α and β as a function of h that are used in the simulation. Future works will deeply investigate other possible types of tuning and settings of $\alpha(h)$ and $\beta(h)$.

Figure 8B shows the PV power (black line) used as an example in the simulation. Since the daily PV generation amount is 1,050 kWh (half of the annual-based daily average), this case study can be classified as a medium-low irradiance scenario. The colored area plots depict the P_{EVs} (aggregate EV power) referring to the standard CMS (light blue), the 1d-OCMS (yellow), and the 2d-OCMS (red)-based SC. In this case, all of the PV energy was exploited for charging; there are no differences among P_{EVs} of the three examined CMSs (intersection area is displayed in green color). On the right-hand axis, the red line depicts the h-coefficient, which remains around low values (about $h = 0.25$), providing a dynamic comparison between the primary source availability versus the EV charging demand.

Figure 9A shows each EV_i charging power referring to the standard CMS (left, blue tint), the 1d-OCMS (center, gray tint), and the 2d-OCMS (right, orange tint). As **Eq. 13** describes, the standard CMS equally allocates each P_{EVi} among plugged vehicles as a function of the PV availability. In other words, as the figure shows, in the case of CMS operation, the reference charging power is the same for each i-th vehicle. On the other hand, **Figure 9A** center and right frames show that the P_{EVi} allocation can be different among vehicles, and it can dynamically change as h varies following A_i (1d-OCMS) and B_i (2d-CMS) evolution. The lower SOC_i, the higher the power provided to EV_i. Furthermore, **Figure 9A** right plot shows the V2V mode

FIGURE 8 | (A) 1d-OCMS setting of the weighting factors $\alpha(h)$ and $\beta(h)$ used in the simulations. **(B)** The daily evolution of h-factor (red line), PV (black line) power, and EVs charging power in case of standard CMS (light blue area), 1d-OCMS (yellow area), and 2d-OCMS (red area). The intersection area (displayed in green color) shows that there are no differences among the three CMSs in this case.

FIGURE 9 | EV population (100 users) charging power profile **(A)** and SOC evolution **(B)** as a function of the time, in case of standard CMS **(left frames, blue tint)**, 1d-OCMS **(center frames, gray tint)**, and 2d-OCMS **(right frames, orange tint)** on a 24 h period. Each line in **(A)** depicts the power value $P_{EVi}(t)$ of a vehicle belonging to the examine 100-user population. Then, each line of **(B)** depicts the $SOC_i(t)$ evolution of the i-th EV.

FIGURE 10 | 31-day SOC_f distribution applying the standard CMS **(A)**, the 1d-OCMS **(B)**, and the 2d-OCMS **(B)**. The right axis shows the average estimated distribution (solid lines). The left axis refers to the scatter plot of the SOC_{fi} (100 users) collected during the 31-day simulation.

operation of 2d-OCMS, when power flows can reverse direction allowing other vehicles to charge at a higher rate. The different allocated charging powers among vehicles influences the EV fleet SOC evolution during the charging process as visible in **Figure 9B**. The same color tones of **Figure 9A** are used to compare the SOC results. The thickest line in each frame depicts the instantaneous average SOC value of the whole EV population. As the figure shows, the same initial SOC (SOC_0) population is assumed for all the CMSs. As expected, different charging power allocations (**Figure 9A**) produce differences in the departure SOC (SOC_f) distributions. In case of charging operated by the standard CMS (**Figure 9B** left frame), SOC_i increases freely. Vehicles that arrive having higher SOC_{0i}, or exhibiting longer parking time, manage to reach a high SOC_{fi}, at the expense of vehicles presenting lower SOC_{0i}, or shorter parking times. On the other hand, the 1d-OCMS and 2d-OCMS shape the SOC_i evolution during the charging process allowing to reach an overall good SOC_{fi} for all the vehicles. The percentage of EVs that present a low-SOC level at departure time is strongly reduced. Differently from 1d-OCMS (**Figure 9B** center frame), through the 2d-OCMS allocation (**Figure 9B** right frame), high-SOC vehicles share power (V2V) with low-SOC vehicles. This phenomenon is witnessed by the nonmonotonous evolution of SOC_i top traces. In this way, in addition to the power share given by PV generation, the latter receive additional power from high-SOC vehicles. In other words, as **Figure 9B** right frame shows, EV with higher SOC starts discharging (SOC decreasing) stimulating faster charging of EV with lower SOC (higher SOC growth rate). It is worth noticing that although the trend of the mean SOC remains approximately the same, the values of the SOC_{fi} population are more concentrated around the average. As a result, the 1d- and 2d-OCMS provide a more homogeneous departure SOC population, decreasing the standard deviation among SOC_{fi}.
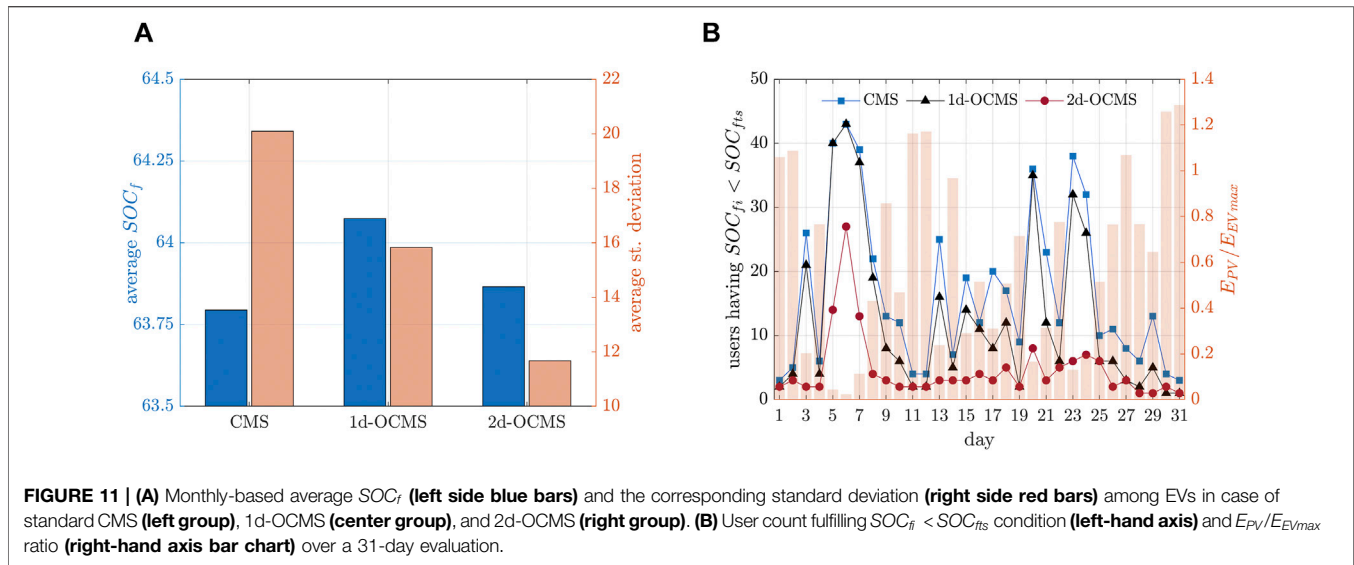
To provide an appreciable statistical significance of the results, the simulation runs considering 31 different days of January (1 month) are carried out. In this condition, the solar irradiation is generally low providing a scenario where the standard CMS's weakness 1 occurs more frequently. The distribution of SOC_{0i} and the parking arrival and departure times are set according to *EV Aggregate Charging Demand Evaluation for a Working Place Parking Lot Scenario* section (**Figure 2** and **Figure 3**, respectively). Based on the same conditions (SOC_{0i}, parking time, and PV power profile), simulations are run by operating the standard CMS, the 1d-OCMS, and the 2d-OCMS SC strategy. Finally, for each day the departure SOC's values, SOC_{fi} (at the end of charging) is collected and analyzed.

Figure 10 shows the SOC_f distribution of the 31 days of January applying the standard CMS, the 1d-OCMS, and the 2d-OCMS, respectively, in **Figures 10A–C**. The right axis shows the 31-day average estimated distribution (solid lines), while the left axis shows the SOC_f scatter plot of each EV_i (100 users/day) collected during the 31-day simulations (3,100 charging events).

The results demonstrate that the two OCMS (1d-OCMS and 2d-OCMS) provide better performance decreasing the number of EVs having a low SOC_f value at the end of charging compared with the standard CMS. In these terms, the best performing method seems to be the 2d-OCMS, which statistically presents the lowest probability in correspondence with low SOC_f values.

Finally, **Figure 11** provides an overview of the 31-day simulation results. **Figure 11A** shows the monthly-based average SOC_f and the corresponding standard deviation among EVs. Although the two OCMSs operate at the expense of EVs with higher SOC, the average SOC_f (the value at the departure time) of the whole EV population does not suffer detrimental effects. On the contrary, as **Figure 11A** shows, the mean value of SOC_f (blue bars, right axis) slightly increases compared to the standard CMS. On the other hand, the results in **Figure 11A** (red bar, right axis) show a much more homogeneous SOC_f population, presenting a lower standard deviation. Compared to the standard CMS, the 1d-OCMS provides a standard deviation diminishing of about 20%, while 2d-OCMS

FIGURE 11 | (A) Monthly-based average SOC_f **(left side blue bars)** and the corresponding standard deviation **(right side red bars)** among EVs in case of standard CMS **(left group)**, 1d-OCMS **(center group)**, and 2d-OCMS **(right group)**. **(B)** User count fulfilling $SOC_{fi} < SOC_{fts}$ condition **(left-hand axis)** and E_{PV}/E_{EVmax} ratio **(right-hand axis bar chart)** over a 31-day evaluation.

(enabling V2V mode) presents a decrease of at least 40%. This trend is reflected in the number of vehicles that leave the parking lot having a medium-low-SOC value. To enumerate the latter, a 37.5% lower threshold (SOC_{fts}) is assumed. This precautionary value represents the minimum SOC level that manages to provide the energy required to cover a 1-day trip (about 30 km), with reference to the EV having the lowest capacity (20 kWh). This evaluation has been done considering the average daily consumption of 5.5 kWh and assuming $SOC_0 = SOC_{min} = 10\%$. In fact, under this hypothesis, an acceptable value of SOC_f (at the departure instant) is

$$SOC_{fts} = 10\% + 100 \frac{5.5 \text{ kWh}}{20 \text{ kWh}} = 37.5\%.$$

In other words, if $SOC_{fi} < SOC_{fts}$ occurs, EV_i has not received enough energy to make the 1-day journey. However, it should be considered that only 20% of the examined EV population has less than 20 kWh of battery capacity and SOC_{fth} is considered as a precautionary threshold. Finally, **Figure 11B** shows the number of users leaving the parking lot having $SOC_{fi} < SOC_{fts}$. The figure shows the count (left-hand axis) considering each day of January (1-month simulation). The blue, black, and red lines refer to the standard CMS, the 1d-OCMS, and the 2d-OCMS, respectively. To quantify the daily PV availability with respect to the EVs' maximum energy demand, the barplot (right-hand axis) reports the ratio between the PV-generated energy and the energy that EVs would require if charged at their maximum power (standard unmanaged G2V charging). The latter corresponds to $E_{EVmax} = 1856$ kWh/d. **Figure 11B** shows that, especially under low PV availability when E_{EVmax} is much higher than E_{PV} (low ratio values), the two OCMS allows more EVs to leave the parking lot with a higher SOC value. Compared to the standard CMS, the 2d-OCMS provides the best results (up to 32 EVs less), followed by the 1d-OCMS (up to 12 EVs less). Based on the monthly average, the 1d-OCMS outpaces standard CMS allowing +36.5% more users

to overpass the SOC_{fts} threshold. This increment rises to +68.9% considering the 2d-OCMS. Finally, under low irradiation conditions (weakness 1) and without requiring power from the external grid, results report that SC operating through the proposed 2d-OCMS, which involves V2V mode, shows the best performance in terms of PV availability exploitation optimization.

In order to compare the 1d-OCMS and 2d-OCMS performance with respect to the standard CMS under medium-high PV irradiance conditions, simulations are run considering the 31 days of May where weakness 2 might occur more frequently. **Figure 12A** shows the daily power flows referring to a scenario in which the PV plant's daily energy generation is about 1900 kWh ($E_{PV}/E_{EVmax} \cong 1$). On the other side, in **Figure 12B**, the PV-generated power during the 24 h is about 50% more than the EV energy demand ($E_{PV}/E_{EVmax} \cong 1.5$). The left-hand axis of both **Figures 12A,B** plots the h-ratio (red line) providing a dynamic comparison between the PV source availability versus the EV charging demand as a function of time. The colored areas depict the aggregate power (and energy) delivered to the whole EV fleet by the three different CMSs. **Figure 12A** shows that especially when the h values are around one, 1d-OCMS and 2d-OCMS manage to better exploit the PV power availability, delivering more energy to the vehicles. Of course, when the h-ratio is much higher than one, the PV power is high enough to provide the maximum power to each EV_i. Therefore, as **Figure 12B** shows, the energy gap between the standard CMS and the two OCMS reduces.

To quantitatively calculate the daily energy gap, defined as $\Delta E_{EV} = E_{EV}^{OCMS} - E_{EV}^{CMS}$, the 31-day simulation results are collected and reported in **Figure 12C**. The right-hand axis shows the ratio E_{PV}/E_{EVmax} referring to the month of May, while on the left axis, the figure shows the 1d-OCMS and 2d-OCMS energy gain (ΔE_{EV}) with respect to the standard CMS. The results show that it is possible to gain up to 80 kWh over

FIGURE 12 | Daily evolution of *h*-factor (red line), PV (black line) power, and EVs charging power in case of standard CMS (light blue area), 1d-OCMS (yellow area), and 2d-OCMS (red area) in case of $E_{PV}/E_{EVmax} \cong 1$ **(A)** and $E_{PV}/E_{EVmax} \cong 1.5$ **(B)**. The intersection area is displayed in green color. **(C)** Daily energy gap ΔE_{EV} **(left-hand axis)** and E_{PV}/E_{EVmax} ratio **(right-hand axis bar chart)** over a 31-day evaluation.

the standard CMS. However, although 2d-OCMS performed better than 1d-OCMS in improving weakness 1, the monthly average ΔE_{EV} is about 30 kWh for both OCMSs. This is due to the similar behavior that **Eqs 18**, **21** based on OCMSs present when $h \geq 1$.

CONCLUSION

In the context of energy districts presenting a growing penetration of RES and EVs, this paper proposed two novel EV charging management systems able to operate in SC mode, suitable for working place parking lots or similar scenarios. Proposed SC positively integrates EV charging with intermittent energy sources by dynamically managing the aggregate EV power demand acting on each vehicle charging power. The CMS pursues local level EV charging maximization

from renewable internal power sources, minimizing consumption from the external grid.

Simulations considering an actual case study validated the effects of the proposal on a reference scenario consisting of an industrial area having a PV plant, non-modulable electrical loads, and EV CS. Based on 24/7/365 data analysis, results demonstrated that SC increases charging self-consumption by 45% on average compared to the standard (G2V) charging. While a 20% reduction in peak power load (measured on PCC, grid side) is experienced as well. However, two main weaknesses emerged. Firstly, EVs' SOC at the instant of departure is particularly low compared to standard G2V counterpart under low availabilities of the primary internal power source. Secondly, PV energy appears to be underutilized due to the equal allocation of PV power among vehicles.

Two novel charging strategies aiming to overcome these two weaknesses are proposed. Both OCMSs ensure an overall good

SOC level at departure time for all the vehicles and maximize the PV power utilization, avoiding the bottleneck phenomenon of the maximum charger rating. The two OCMS differs as a function of the power flow direction. The 1d-OCMS only considers the PV to EV flows direction (standard SC). On the other hand, the 2d-OCMS enables bidirectional power flow among EVs (V2V). Simulations carried out in conditions where these weaknesses are more highlighted showed improvements of 36.5% (1d-OCMS) and 68.9% (2d-OCMS) in the number of users presenting a departure SOC suitable for covering a 1-day trip under medium-low irradiance scenarios, considering that medium-high irradiance scenarios 1d- and 2d-OCMS present similar performances. Both techniques managed to provide up to 80 kW h/d more than the standard CMS (+30 kWh on average). Most performing results in terms of SOC distribution are achieved by operating the 2d-OCMS. Thanks to the bidirectional V2V mode, an average decrease of 40% in SOC standard deviation at the departure instant has been achieved. If suitable, 2d-OCMS should be preferred because of its ability to obtain a homogeneous charging process and overall better performance in all investigated scenarios. However, in case conventional unidirectional charging operations are required, 1d-OCMS should be preferred because of the shown improvements in comparison to the standard CMS.

DATA AVAILABILITY STATEMENT

The original contributions presented in the study are included in the article/Supplementary Material; further inquiries can be directed to the corresponding author.

AUTHOR CONTRIBUTIONS

All authors listed have made a substantial, direct, and intellectual contribution to the work and approved it for publication.

FUNDING

REFERENCES

Aldik, A., and Khatib, T. (2019). EV Aggregators and Energy Storage Units Scheduling into Ancillary Services Markets: The Concept and Recommended Practice. *Wevj* 11, 8. doi:10.3390/wevj11010008

Bernards, R., van Westering, W., Morren, J., and Slootweg, H. (2020). Analysis of Energy Transition Impact on the Low-Voltage Network Using Stochastic Load and Generation Models. *Energies* 13, 6097. doi:10.3390/en13226097

Bons, P. C., Buatois, A., Ligthart, G., Geerts, F., Piersma, N., and van den Hoed, R. (2020). Impact of Smart Charging for Consumers in a Real World Pilot. *Wevj* 11, 21. doi:10.3390/wevj11010021

Bovera, F., Gabba, M., and Zatti, M. (2021). An Optimization Model for the Provision of Flexibility and Dispatching Resources by Multi-Vector Smart Energy Districts. *E3s Web Conf.* 238, 05007. doi:10.1051/e3sconf/202123805007

Branco, N. C., and Affonso, C. M. (2020). Probabilistic Approach to Integrate Photovoltaic Generation into Pevs Charging Stations Considering Technical, Economic and Environmental Aspects. *Energies* 13, 5086. doi:10.3390/en13195086

Directorate-General for Climate Action (European Commission) (2019). *Going Climate-Neutral by 2050 - A Strategic Long-Term Vision for a Prosperous, Modern, Competitive and Climate-Neutral EU Economy.* Luxembourg: Publications Office of the European Union. doi:10.2834/02074

Dogan, A., Kuzlu, M., Pipattanasomporn, M., Rahman, S., and Yalcinoz, T. (2015). "Impact of EV Charging Strategies on Peak Demand Reduction and Load Factor Improvement," in 2015 9th International Conference on Electrical and Electronics Engineering (ELECO), Bursa, Turkey, November 26–28, 2015 (IEEE), 374–378. doi:10.1109/ELECO.2015.7394559

European Alternative Fuel Observatory - EAFO (2021). Available at: https://www.eafo.eu/ (Accessed March 6, 2021).

Ev database (2021). EV Database Compare Electric Vehicles. Available at: https://ev-database.org/ (Accessed March 16, 2021).

Fachrizal, R., and Munkhammar, J. (2020). Improved Photovoltaic Self-Consumption in Residential Buildings with Distributed and Centralized Smart Charging of Electric Vehicles. *Energies* 13, 1153. doi:10.3390/en13051153

Ferreira, J. C., Monteiro, V., and Afonso, J. L. (2014). Vehicle-to-anything Application (V2Anything App) for Electric Vehicles. *IEEE Trans. Ind. Inf.* 10, 1927–1937. doi:10.1109/TII.2013.2291321

Fouladi, E., Baghaee, H. R., Bagheri, M., and Gharehpetian, G. B. (2020). Power Management of Microgrids Including PHEVs Based on Maximum Employment of Renewable Energy Resources. *IEEE Trans. Ind. Applicat.* 56, 5299–5307. doi:10.1109/TIA.2020.3010713

Hasan, E., Sharma, S., and Brenna, M. (2019). "Virtual Energy Storage System Using Aggregated Electric Vehicles for Ancillary Services in Distribution Grid," in 2019 AEIT International Conference of Electrical and Electronic Technologies for Automotive, AEIT AUTOMOTIVE 2019, Turin, Italy, July 2–4, 2019 (Institute of Electrical and Electronics Engineers Inc.). doi:10.23919/EETA.2019.8804570

Heinisch, V., Göransson, L., Erlandsson, R., Hodel, H., Johnsson, F., and Odenberger, M. (2021). Smart Electric Vehicle Charging Strategies for Sectoral Coupling in a City Energy System. *Appl. Energ.* 288, 116640. doi:10.1016/j.apenergy.2021.116640

Hinterberger, R., Gollner, C., Noll, M., Meyer, S., and Schwarz, H.-G. (2020). White Paper on PED Reference Framework White Paper on Reference Framework for Positive Energy Districts and Neighbourhoods. Vienna, Austria. Available at: https://jpi-urbaneurope.eu/ped/ (Accessed April 2, 2021).

IEC 62196-1 TC 23/SC 23H (2014). *IEC 62196-1 Plugs, Socket-Outlets, Vehicle Connectors and Vehicle Inlets - Conductive Charging of Electric Vehicles - Part 1: General Requirements.* IEC. Available at: https://webstore.iec.ch/publication/6582 (Accessed March 10, 2021).

Kroposki, B., Johnson, B., Zhang, Y., Gevorgian, V., Denholm, P., Hodge, B.-M., et al. (2017). Achieving a 100% Renewable Grid: Operating Electric Power Systems with Extremely High Levels of Variable Renewable Energy. *IEEE Power Energ. Mag.* 15, 61–73. doi:10.1109/MPE.2016.2637122

Lo Franco, F., Ricco, M., Mandrioli, R., and Grandi, G. (2020). Electric Vehicle Aggregate Power Flow Prediction and Smart Charging System for Distributed Renewable Energy Self-Consumption Optimization. *Energies* 13, 5003. doi:10.3390/en13195003

Lo Franco, F., Morandi, A., Raboni, P., and Grandi, G. (2021a). Efficiency Comparison of DC and AC Coupling Solutions for Large-Scale PV+BESS Power Plants. *Energies* 14, 4823. doi:10.3390/en14164823

Franco, F. L., Ricco, M., Mandrioli, R., Paternost, R. F. P., and Grandi, G. (2021b). "State of Charge Optimization-Based Smart Charging of Aggregate Electric

Vehicles from Distributed Renewable Energy Sources," in 2021 IEEE 15th International Conference on Compatibility, Power Electronics and Power Engineering, Florence, Italy, July 14–16, 2021 (CPE-POWERENG, IEEE), 1–6. doi:10.1109/CPE-POWERENG50821.2021.9501214

Lopes, J. A. P., Soares, F. J., and Almeida, P. M. R. (2011). Integration of Electric Vehicles in the Electric Power System. *Proc. IEEE* 99, 168–183. doi:10.1109/JPROC.2010.2066250

Lopes, R. A., Martins, J., Aelenei, D., and Lima, C. P. (2016). A Cooperative Net Zero Energy Community to Improve Load Matching. *Renew. Energ.* 93, 1–13. doi:10.1016/j.renene.2016.02.044

Luo, C., and Ooi, B.-T. (2006). Frequency Deviation of Thermal Power Plants Due to Wind Farms. *IEEE Trans. Energ. Convers.* 21, 708–716. doi:10.1109/TEC.2006.874210

Mao, T., Zhang, X., and Zhou, B. (2018). Modeling and Solving Method for Supporting 'Vehicle-To-Anything' EV Charging Mode. *Appl. Sci.* 8, 1048. doi:10.3390/APP8071048

Mirbagheri, S. M., Bovera, F., Falabretti, D., Moncecchi, M., Delfanti, M., Fiori, M., and Merlo, M. (2018). "Monte Carlo Procedure to Evaluate the E-Mobility Impact on the Electric Distribution Grid," in 2018 International Conference of Electrical and Electronic Technologies for Automotive, AUTOMOTIVE 2018, Milan, Italy, July 9–11, 2018 (Institute of Electrical and Electronics Engineers Inc.). doi:10.23919/EETA.2018.8493169

Monteiro, V., Pinto, J. G., and Afonso, J. L. (2016). Operation Modes for the Electric Vehicle in Smart Grids and Smart Homes: Present and Proposed Modes. *IEEE Trans. Veh. Technol.* 65, 1007–1020. doi:10.1109/TVT.2015.2481005

Nelder, C., and Fitzgerald, G. (2016). Electric Vehicles as Distributed Energy Resources. Available at: https://www.researchgate.net/publication/324417842_Electric_Vehicles_as_Distributed_Energy_Resources (Accessed March 8, 2021).

Noel, L., Zarazua de Rubens, G., Kester, J., and Sovacool, B. K. (2019). *Vehicle-to-Grid.* Cham: Springer International Publishing. doi:10.1007/978-3-030-04864-8

Noel, L., Zarazua de Rubens, G., Kester, J., and Sovacool, B. K. (2021). Leveraging User-Based Innovation in Vehicle-To-X and Vehicle-To-Grid Adoption: A Nordic Case Study. *J. Clean. Prod.* 287, 125591. doi:10.1016/j.jclepro.2020.125591

Pearre, N. S., and Ribberink, H. (2019). Review of Research on V2X Technologies, Strategies, and Operations. *Renew. Sustain. Energ. Rev.* 105, 61–70. doi:10.1016/j.rser.2019.01.047

Rakhshani, E., Rouzbehi, K., J. Sánchez, A. A., Tobar, A. C., and Pouresmaeil, E. (2019). Integration of Large Scale PV-Based Generation into Power Systems: A Survey. *Energies* 12, 1425. doi:10.3390/en12081425

Ramadhani, U. H., Fachrizal, R., Shepero, M., Munkhammar, J., and Widén, J. (2021). Probabilistic Load Flow Analysis of Electric Vehicle Smart Charging in Unbalanced LV Distribution Systems with Residential Photovoltaic Generation. *Sustain. Cities Soc.* 72, 103043. doi:10.1016/j.scs.2021.103043

Rancilio, G., Bovera, F., and Delfanti, M. (2021). "A Techno-Economic Evaluation of the Impact of Electric Vehicles Diffusion on Italian Customer Billing Tariffs. *E3s Web Conf.* 238, 07003. doi:10.1051/e3sconf/202123807003

Tanguy, K., Dubois, M. R., Lopez, K. L., and Gagné, C. (2016). Optimization Model and Economic Assessment of Collaborative Charging Using Vehicle-To-Building. *Sustain. Cities Soc.* 26, 496–506. doi:10.1016/j.scs.2016.03.012

Thingvad, A., Martinenas, S., Andersen, P. B., Marinelli, M., Olesen, O. J., and Christensen, B. E. (2016). "Economic Comparison of Electric Vehicles Performing Unidirectional and Bidirectional Frequency Control in Denmark with Practical Validation," in 2016 51st International Universities Power Engineering Conference (UPEC), Coimbra, Portugal, September 6–9, 2016 (IEEE), 1–6. doi:10.1109/UPEC.2016.8113988

Thompson, A. W., and Perez, Y. (2020). Vehicle-to-Everything (V2X) Energy Services, Value Streams, and Regulatory Policy Implications. *Energy Policy* 137, 111136. doi:10.1016/J.ENPOL.2019.111136

Thompson, A. W. (2018). Economic Implications of Lithium Ion Battery Degradation for Vehicle-To-Grid (V2X) Services. *J. Power Sourc.* 396, 691–709. doi:10.1016/j.jpowsour.2018.06.053

Tuominen, P. (2020). Yes to Positive Energy Districts. Available at: https://www.vttresearch.com/en/news-and-ideas/yes-positive-energy-districts-how-make-it-happen (Accessed March 21, 2021).

Ul-Haq, A., Cecati, C., and El-Saadany, E. (2018). Probabilistic Modeling of Electric Vehicle Charging Pattern in a Residential Distribution Network. *Electric Power Syst. Res.* 157, 126–133. doi:10.1016/j.epsr.2017.12.005

UNRAE (2020). *Top 10 Per Alimentazione - Dicembre 2019.* UNRAE, 1–2. Available at: http://www.unrae.it/dati-statistici/immatricolazioni/4831/top-10-per-alimentazione-dicembre-2019 (Accessed March 16, 2021).

Wang, Q., Liu, X., Du, J., and Kong, F. (2016). Smart Charging for Electric Vehicles: A Survey from the Algorithmic Perspective. *IEEE Commun. Surv. Tutorials* 18, 1500–1517. doi:10.1109/COMST.2016.2518628

Yamagata, Y., Seya, H., and Kuroda, S. (2014). Energy Resilient Smart Community: Sharing Green Electricity Using V2C Technology. *Energ. Proced.* 61, 84–87. doi:10.1016/j.egypro.2014.11.912

Zatti, M., Martelli, E., and Amaldi, E. (2017). "A Three-Stage Stochastic Optimization Model for the Design of Smart Energy Districts under Uncertainty," in *27th European Symposium on Computer Aided Process Engineering. Computer Aided Chemical Engineering* (Amsterdam: Elsevier B.V.), 2389–2394. doi:10.1016/B978-0-444-63965-3.50400-1

Zipf, M., and Most, D. (2016). "Cooperation of TSO and DSO to Provide Ancillary Services," in 2016 13th International Conference on the European Energy Market (EEM), Porto, Portugal, June 6–9, 2016 (IEEE), 1–6. doi:10.1109/EEM.2016.7521273